



HAL
open science

Hippocampal Egr1 -Dependent Neuronal Ensembles Negatively Regulate Motor Learning

Verónica Brito, Enrica Montalban, Anna Sancho-Balsells, Anika Pupak,
Francesca Flotta, Mercè Masana, Silvia Ginés, Jordi Alberch, Claire Martin,
Jean-Antoine Girault, et al.

► **To cite this version:**

Verónica Brito, Enrica Montalban, Anna Sancho-Balsells, Anika Pupak, Francesca Flotta, et al.. Hippocampal Egr1 -Dependent Neuronal Ensembles Negatively Regulate Motor Learning. *Journal of Neuroscience*, 2022, 42 (27), pp.5346-5360. 10.1523/JNEUROSCI.2258-21.2022 . hal-03968267

HAL Id: hal-03968267

<https://hal.science/hal-03968267>

Submitted on 7 Mar 2023

HAL is a multi-disciplinary open access archive for the deposit and dissemination of scientific research documents, whether they are published or not. The documents may come from teaching and research institutions in France or abroad, or from public or private research centers.

L'archive ouverte pluridisciplinaire **HAL**, est destinée au dépôt et à la diffusion de documents scientifiques de niveau recherche, publiés ou non, émanant des établissements d'enseignement et de recherche français ou étrangers, des laboratoires publics ou privés.

73 **Hippocampal *Egr1*-dependent neuronal ensembles negatively**
74 **regulate motor learning**

75

76 Abbreviated title: Hippocampal *Egr1* in motor learning

77

78 Verónica Brito^{1,2,3*}, Enrica Montalban⁴, Anna Sancho-Balsells^{1,2,3}, Anika
79 Pupak^{1,2,3}, Francesca Flotta^{1,2,3}, Mercè Masana^{1,2,3}, Silvia Ginés^{1,2,3}, Jordi
80 Alberch^{1,2,3,5}, Claire Martin⁴, Jean-Antoine Girault^{6,7,8} and Albert Giralt^{1,2,3,5,*}

81

82 ¹Departament de Biomedicina, Facultat de Medicina, Institut de Neurociències,
83 Universitat de Barcelona, Barcelona. CP: 08036 Spain.

84 ²Institut d'Investigacions Biomèdiques August Pi i Sunyer (IDIBAPS), Barcelona.
85 CP: 08036. 13 Spain.

86 ³Centro de Investigación Biomédica en Red sobre Enfermedades
87 Neurodegenerativas 15 (CIBERNED), Spain.

88 ⁴Université de Paris, BFA, UMR 8251, CNRS, F-75014 Paris, France.

89 ⁵Production and Validation Center of Advanced Therapies (Creatio), Faculty of
90 Medicine and 18 Health Science, University of Barcelona, 08036 Barcelona, Spain
91 19

92 ⁶Inserm UMR-S 1270, 75005 Paris, France.

93 ⁷Sorbonne Université, Science and Engineering Faculty, 75005 Paris, France. 21

94 ⁸Institut du Fer a Moulin, 75005 Paris, France.

95

96 Correspondence to: **Albert Giralt** or **Veronica Brito**, Departament de
97 Biomedicina, Facultat de Medicina, Institut de Neurociències, Universitat de
98 Barcelona, Barcelona 08036, Spain. E25 mail: albertgiralt@ub.edu,
99 veronica.brito@ub.edu.

100 **Acknowledgements**

101 AG is a Ramón y Cajal fellow (RYC-2016-19466). AG (RTI2018-094678-A-I00),
102 SG

103 (RTI2018-094374-B-I00), JA (PID2020-119386RB-100) and VB (PID2020-
104 116474RB36 I00) were supported by grants from Ministerio de Ciencia, Innovación
105 y Universidades. 37 We thank Ana López (María de Maeztu Unit of Excellence,
106 Institute of Neurosciences, 38 University of Barcelona, MDM-2017-0729, Ministry
107 of Science, Innovation and 39 Universities) for technical support. We thank María
108 Calvo from the Advanced 40 Microscopy Service (Centres Científics i Tecnològics
109 Universitat de Barcelona) for her 41 help in the acquisition, analysis, and
110 interpretation of the confocal images. We also 42 thank to Daniel del Toro and
111 Eulàlia Martí, from the Institut de Neurociències, for their 43 insightful comments
112 and advice.

113

114 **Competing interests**

115 The authors declare no competing financial interests.

116 **Abstract**

117 Motor skills learning is classically associated with brain regions including cerebral
118 and cerebellar cortices and basal ganglia nuclei. Less is known about the role of
119 the hippocampus in the acquisition and storage of motor skills. Here we show that
120 mice receiving a long-term training in the accelerating rotarod display marked
121 hippocampal transcriptional changes and reduced pyramidal neurons activity in the
122 CA1 region when compared with naïve mice. Then, we use mice in which neural
123 ensembles are permanently labeled in an *Egr1* activity-dependent fashion. Using
124 these mice, we identify a subpopulation of *Egr1*-expressing pyramidal neurons in
125 CA1 activated in short- and long-term trained mice in the rotarod task. When *Egr1*
126 is downregulated in the CA1 or these neuronal ensembles are depleted, motor
127 learning is improved whereas their chemogenetic stimulation impairs motor
128 learning performance. Thus, *Egr1* organizes specific CA1 neuronal ensembles
129 during the accelerating rotarod task that limit motor learning. These evidences
130 highlight the role of the hippocampus in the control of this type of learning and we
131 provide a possible underlying mechanism.

132

133 **Significance statement**

134 It is a major topic in neurosciences the deciphering of the specific circuits
135 underlying memory systems during the encoding of new information. However, the
136 potential role of the hippocampus in the control of motor learning and the
137 underlying mechanisms has been poorly addressed. In the present work we show
138 how the hippocampus responds to motor learning and how the *Egr1* molecule is
139 one of the major responsible for such phenomenon controlling the rate of motor
140 coordination performances.

141 Introduction

142 It is now well established that the hippocampus is involved in the formation of
143 detailed cognitive ‘maps’ of the context in which learning occurs (Spiers, 2020).
144 However, in addition to its classical role in spatial maps formation, the
145 hippocampus is also involved in tasks that primarily rely on other brain regions. For
146 example, the hippocampus is activated during goal-directed behaviors and
147 strategies (Fidalgo et al., 2012; Palombo et al., 2019) and modulates contextual
148 associations during drug-of-abuse administration (Sjulson et al., 2018; Zhou et al.,
149 2019) or appetitive conditioning (Ito et al., 2008). Despite these previous reports,
150 the role of the hippocampus in motor learning and the underlying mechanisms
151 remain poorly explored. Understanding the implications of the hippocampus in the
152 regulation of motor learning could help to decipher the alterations in neural circuits
153 of complex motor diseases such as Huntington’s and/or Parkinson’s disease in
154 which a severe hippocampal atrophy and/or dysfunction have already been
155 described (Spargo et al., 1993; Camicioli et al., 2003; Calabresi et al., 2013; Begeti
156 et al., 2016; Harris et al., 2019).

157 Potential contributions of the hippocampus to motor learning and coordination
158 have been proposed on the basis of human studies and imaging approaches
159 (Albouy et al., 2013). Cooperative or competitive interactions between the human
160 hippocampus and other brain regions such as the striatum or motor cortex seem
161 to coordinate and synchronize during the acquisition of motor abilities (Albouy et
162 al., 2008; Döhring et al., 2017; Boutin et al., 2018), but the underlying molecular
163 mechanisms and the neural ensembles involved remain unknown. In this line,
164 although initial animal studies with acute hippocampal lesions showed
165 improvements in cued-learning (Lee et al., 2008) or object recognition memory
166 (Oliveira et al., 2010), they did not support a role of the hippocampus in the
167 regulation of motor skills (Curlik et al., 2013; Fouquet et al., 2013). In contrast,
168 neuroimaging approaches have shown that the hippocampus displays higher rates
169 of micro-structural changes in rotarodtrained mice compared to untrained controls
170 and, accordingly, this brain region is larger in the best performers (Scholz et al.,
171 2015). Furthermore, the accelerating rotarod task induces Fos expression (a
172 marker of neural activation) labeling (Nagai et al., 2017), mTOR and cAMP-
173 dependent protein kinase expression (Bergeron et al., 2014; Chagniel et al., 2014),
174 and neurogenesis (DiFeo et al., 2015) in the hippocampus. These observations
175 indicate that the hippocampus is recruited and likely to play a role in the modulation
176 of motor skills learning.

177 In the present work we show major hippocampal transcriptional changes in long-
178 term trained mice in the accelerating rotarod task when compared with untrained
179 mice. Transcriptional profiling reveals the importance of changes in hippocampal
180 synaptic genes during motor learning. Accordingly, the

181 hippocampal CA1 progressively stabilizes and decreases its activity along trials.
182 We then used transgenic mice to tag neuronal ensembles in CA1 in a
183 *Egr1*dependent fashion and show that depletion of such neural populations

184 improves motor learning whereas their chemogenetic activation has a selective
185 negative impact. Thus, our results reveal the existence of hippocampal neuronal
186 ensembles that tightly modulate the rates of motor skills learning.

187

188 **Methods**

189 **Animals**

190 For this study we used adult (12-week old) C57/BL6 males (MGI Cat# 5657800,
191 RRID:MGI:5657800) in experiments related with fiber photometry, RNAseq
192 analyses and *Egr1* downregulation. For the rest of the experiments we used the
193 *Egr1*-CreER^{T2} mice (Longueville et al., 2021). These mice carry a bacterial artificial
194 chromosome (BAC) including the *Egr1* gene in which the coding sequence was
195 replaced by that of CreER^{T2} fusion protein. *Egr1*-CreER^{T2} mice were used as
196 heterozygous in the chemogenetic experiments or they were crossed with R26^{RCE}
197 mice ((Gt(ROSA)26Sor^{tm1.1(CAG-EGFP)^{Fsh}/Mmjax, Strain}

198 004077, The Jackson Laboratory), which harbor the R26R CAG-boosted EGFP
199 (RCE) reporter allele with a loxP-flanked STOP cassette upstream of the enhanced
200 green fluorescent protein (EGFP) gene)) to create the double heterozygous mutant
201 *Egr1*-CreER^{T2} x R26^{RCE} mice for the experiments related with characterization of
202 neural populations or depletion of neural ensembles. Genotypes were determined
203 from an ear biopsy as described elsewhere (Martín-Ibáñez et al., 2012). For
204 genotyping of the Cre and EGFP transgenes we used standard PCR assays
205 following Jackson Laboratory© manufacturer's instructions. All mice were housed
206 together in numerical birth order in groups of mixed genotypes (3–5 mice per
207 cage). The animals were housed with access to food and water *ad libitum* in a
208 colony room kept at 19–22 °C and 40–60% humidity, under an inverted 12:12 h
209 light/dark cycle (from 08:00 to 20:00). All animal procedures were approved by
210 local committees [Universitat de

211 Barcelona, CEEA (133/10); Generalitat de Catalunya (DAAM 5712)] and Animal
212 Care Committee of the University of Paris (APAFIS # 15638)], in accordance with
213 the European Communities Council Directive (86/609/EU).

214 **Stereotaxic surgery and viral transduction in vivo**

215 Animals were stereotaxically injected with one of the following adenoassociated
216 viruses (AAV): AAV-flex-taCasp3-TEVp (UNC vector core); AAV-U6shRNA-*Egr1*-
217 mCherry (#shAAV-258146, Vector Biolabs), AAV-U6-ScramblemCherry (#1781,
218 Vector Biolabs), AAV-CAG-FLEX-tdTomato (UNC vector core) and pAAV-hSyn-
219 DIO-hM3D(Gq)-mCherry (RRID:Addgene_44361). Briefly, mice were
220 anaesthetized with ketamine-xylazine (100 mg/kg and 10mg/kg

221 respectively), and bilaterally injected with AAVs (~2.6 x 10⁹ GS per injection) in the
222 CA1 of the dorsal hippocampus, from the bregma (millimeters); anteroposterior, –
223 2.0; lateral, ±1.5; and dorso-ventral, -1.3. AAV injection was carried out in 2 min.
224 The needle was left in place for 7 min for complete virus diffusion before being

225 slowly pulled out of the tissue. After 2 h of careful monitoring, mice were returned
226 to their home cage for 3 weeks. All mice subjected to surgery that survived and
227 were healthy without clinical problems (such as head inclination or >15% of body
228 weight loss) were also behaviorally characterized. Once the behavioral
229 characterization was done, half of the brain was used to verify the site of
230 injection by immunofluorescence (see *Tissue fixation, immunofluorescence's*
231 section). Mice that showed no correct viral transduction and location were excluded
232 from the entire study.

233

234 **Pharmacological treatments**

235 We used single intra-peritoneal injections of 4-hydroxytamoxifen (4-HT, Sigma,
236 #H7904) 50 mg/kg or clozapine-N-oxide (CNO, Sigma, #C0832) 3 mg/kg. The 4-
237 HT's vehicle was peanut oil (Sigma, #2144) (with a previous dissolution by heating
238 in 100% EtOH) and for CNO was distilled water. 4-HT was always administered 1
239 h prior to the behavioral testing and CNO was always administered 30 min prior to
240 the behavioral testing or 2 h prior to the mice sacrifice and brain tissue collection.

241 **Fiber photometry**

242 Male C57BL/6 mice were anaesthetized with isoflurane and received 10 mg.kg⁻¹
243 intraperitoneal injection (i.p.) of Buprécare® (buprenorphine 0.3 mg) diluted 1/100
244 in NaCl 9 g.L⁻¹ and 10 mg.kg⁻¹ of Ketofen® (ketoprofen 100 mg) diluted 1/100 in
245 NaCl 9 g.L⁻¹, and placed on a stereotactic frame (Model 940, David Kopf
246 Instruments, California). 1 µL of virus AAV9.CamKII.GCaMP6f.WPRE.SV40, titer
247 $\geq 1 \times 10^{13}$ vg/mL, working dilution 1:10), was injected unilaterally into the CA1 (L =
248 -1.25; AP = -2; V = -1.1-1.2, in mm) at a rate of 0.1 µL.min⁻¹.
249 pENN.AAV.CamKII.GCaMP6f.WPRE.SV40 was a gift from James M. Wilson
250 (Addgene viral prep # 100834-AAV9). A chronically implantable cannula (Doric
251 Lenses, Québec, Canada) composed of a bare optical fiber (400 µm core, 0.48
252 N.A.) and a fiber ferrule was implanted at the location of the viral injection site. The
253 fiber was fixed onto the skull using dental cement (Super-Bond C&B, Sun Medical).
254 Real time fluorescence emitted from GCaMP6f-expressing neurons was recorded
255 using fiber photometry as described (Berland et al., 2020). Fluorescence was
256 collected using a single optical fiber for both delivery of excitation light streams and
257 collection of emitted fluorescence. The fiber photometry setup used 2 lightemitting
258 LEDs: 405 nm LED sinusoidally modulated at 330 Hz and a 465 nm LED
259 sinusoidally modulated at 533 Hz (Doric Lenses) merged in a FMC4 MiniCube
260 (Doric Lenses) that combines the 2 wavelengths excitation light streams and
261 separate them from the emission light. The MiniCube was connected to a
262 Fiberoptic rotary joint (Doric Lenses) connected to the cannula. A RZ5P lock-in
263 digital processor controlled by the Synapse software (TuckerDavis Technologies,
264 TDT, USA), commanded the voltage signal sent to the emitting LEDs via the LED
265 driver (Doric Lenses). The light power before entering the implanted cannula was
266 measured with a power meter (PM100USB, Thorlabs) before the beginning of each

267 recording session. The irradiance was ~ 9 mW/cm². The fluorescence emitted by
268 GCaMP6f in response to light excitation was collected by a femtowatt
269 photoreceiver module (Doric Lenses) through the same fiber patch cord. The signal
270 was received by the RZ5P processor (TDT). Real time fluorescence due to 405-
271 nm and 465-nm excitations was demodulated online by the Synapse software
272 (TDT). A camera was synchronized with the recording using the Synapse software.
273 Signals were exported to MATLAB R2016b (Mathworks) and analyzed offline. After
274 careful visual examination of all trials, they were clean of artifacts in these time
275 intervals. The timing of events was extracted from the video. To calculate $\Delta F/F$, a
276 linear least-squares fit was applied to the 405 nm signal to align it to the 465 nm
277 signal, producing a fitted 405 nm signal. This was then used to normalize the 465
278 nm signal as follows: $\Delta F/F = (465 \text{ nm signal} - \text{fitted } 405 \text{ nm signal})/\text{fitted } 405 \text{ nm}$
279 signal (Lerner et al., 2015). For each trial, signal analysis was performed from -10
280 to +20 sec around the moment the mouse is positioned on the rotarod. The
281 percentage of change of the AUC was calculated between [-10 0] and [0 10]sec
282 relative to the moment when animals were placed in the from rotarod.

283 **Accelerating rotarod**

284 As previously described (Giralt et al., 2013), animals were placed on a motorized
285 rod (30-mm diameter, Panlab, Spain). The rotation speed was gradually increased
286 from 4 to 40 r.p.m. over the course of 5 min. The fall latency time was recorded
287 when the animal was unable to keep up with the increasing speed and fell. Rotarod
288 training/testing was performed 4 times per day with 30 min as inter-trial time
289 interval. The results show the average of fall latencies per trial during the five days
290 of training. In experiments depicted in figures 1, 3 and 5 we used three groups, a
291 non-trained mice but exposed to the rotarod for 1 day, the short-term trained mice
292 (STT) exposed to only one day of training in the rotarod; and the long-term trained
293 mice (LTT) exposed to five days of training in the rotarod.

294 **Open field and novel object location test**

295 For the novel object location test (NOL), an open-top arena (45 × 45 × 45 cm) with
296 visual cues surrounding the apparatus was used. Mice were first habituated to the
297 arena (1 day, 30 min). We considered this first exposition to the open arena as an
298 open field paradigm. We monitored total traveled distance, time spent in the center
299 of the arena and parallel index as measures of locomotor activity, anxiogenic
300 behavior and spatial navigation strategies respectively. On day 2, two identical
301 objects (A1 and A2) were placed in the arena and explored for 10 min. Twenty-four
302 hour later (Day 3), one object was moved from its original location to the diagonally
303 opposite corner and mice were allowed to explore the arena for 5 min. The object
304 preference was measured as the time exploring each object × 100/time exploring
305 both objects. Behavioral data was processed and analyzed using the Smart Junior
306 software (Panlab, Spain).

307

308 RNA sequencing analysis

309 RNA Extraction and Quality Control. Hippocampal were homogenized, and RNA
310 extracted using RNeasy Lipid Tissue Mini kit (Quiagen) according to
311 manufacturer's recommendations. RNA purity and quantity were determined with
312 a UV/V spectrophotometer (Nanodrop 1000), while RNA integrity was assessed
313 with a 2100 Bioanalyzer (Agilent Technologies Inc., CA), according to
314 manufacturers' protocols. The average RIN value for our samples was 9.5, and the
315 RIN cut-off for sample inclusion was 8.0.

316 RNA Sequencing and Differential Gene Expression Analysis. Libraries were
317 prepared using the TruSeq Stranded mRNA Sample Prep Kit v2 (ref. RS-
318 1222101/2) according to the manufacturer's protocol. Briefly, 500 ng of total RNA
319 were used for poly(A)-mRNA selection using streptavidin-coated magnetic beads
320 and were subsequently fragmented to approximately 300 bp. cDNA was
321 synthesized using reverse transcriptase (SuperScript II, ref. 18064-014, Invitrogen)
322 and random primers. The second strand of the cDNA incorporated dUTP in place
323 of dTTP. Double-stranded DNA was further used for library preparation. dsDNA
324 was subjected to A-tailing and ligation of the barcoded Truseq adapters. Library
325 amplification was performed by PCR using the primer cocktail supplied in the kit.
326 All purification steps were performed using AMPure XP beads. Final libraries were
327 analyzed using Fragment Analyzer to estimate the quantity and check size
328 distribution and were then quantified by qPCR using the KAPA Library
329 Quantification Kit (ref. KK4835, KapaBiosystems) prior to amplification with
330 Illumina's cBot. Sequencing was done using the HiSeq2500 equipment (illumina),
331 Single Read, 50bp, using the v4 chemistry. The quality of the sequencing data was
332 checked using the FastQC software v0.11.5. Andrews S. (2010). FastQC: a quality
333 control tool for high throughput sequence data. Available online at:
334 <http://www.bioinformatics.babraham.ac.uk/projects/fastqc>. An estimation of
335 ribosomal RNA in the raw data was obtained using riboPicker version 0.4.3
336 (Schmieder et al., 2012). Reads were aligned to the GENCODE version of the *Mus*
337 *musculus* genome, release M20 (GRMm38/mm10 assembly) using the STAR
338 mapper (version 2.5.3a) (Dobin et al., 2013). The raw read counts per gene was
339 also obtained using STAR (--quantMode TranscriptomeSAM GeneCounts option)
340 and the GENCODE release M20 annotation
341 ([ftp://ftp.ebi.ac.uk/pub/databases/gencode/Gencode_mouse/release_M20/genc](ftp://ftp.ebi.ac.uk/pub/databases/gencode/Gencode_mouse/release_M20/gencode.vM20.annotation.gtf.gz)
342 [ode.vM20.annotation.gtf.gz](ftp://ftp.ebi.ac.uk/pub/databases/gencode/Gencode_mouse/release_M20/gencode.vM20.annotation.gtf.gz)). The R/Bioconductor package DESeq2 version 1.22.2
343 (R version 3.5.0) was used to assess the differentially expressed genes between
344 experimental groups, using the Wald statistical test and the False Discovery Rate
345 for the p-value correction. Prior to the differential expression analysis, genes with
346 the sum of raw counts across all samples below 10 were discarded, the library
347 sizes were normalized using the default DeSeq2 method, and the read counts were
348 log₂ transformed. To exclude false positive genes, genes with low expression
349 levels (baseMean <10) were excluded from the list of DEGs. Sequencing data has

350 been deposited in NCBI's Gene Expression Omnibus and are accessible through
351 GEO Series accession number (Accession number pending).

352 Gene Functional Enrichment Analysis Metascape pathway enrichment analysis
353 was performed to explore the functional roles of DEGs in the paired comparison of
354 Long-term trained, short-term trained and non-trained mice. To discover further
355 possible connections between DEGs and transcription factors we used EnrichR.
356 Functional annotations for modules of interest were generated using the web
357 server SynGO (<https://www.syngoportal.org/>), which provides an expert-curated
358 resource for synapse function and gene enrichment analysis (Koopmans et al.,
359 2019).

360

361 **Quantitative RT-PCR**

362 The cDNA synthesis was performed at 37 °C for 15 min and a final step at 85 °C
363 for 5 s in a final volume of 20 µl according to the manufacturer's instructions. The
364 cDNA was then analyzed by quantitative RT-PCR using the following PrimeTime
365 qPCR Assays (Integrated DNA Technologies, Inc.): Arc (Mm.PT.58.5865502.g),
366 Mdga1 (Mm.PT.58.32475502), Egr-1 (Mm.PT.58.29064929), Mdga2
367 (Mm.PT.58.10917976), Tnik1 (Mm.PT.58.32835672), Gsgl1
368 (Mm.PT.58.28965348) and Actinβ (Mm.PT.39a.22214843.g). Quantitative PCR
369 was performed in 12µl of final volume on 96-well plates using the Premix Ex Taq
370 (Probe qPCR) (TAKARA BIOTECHNOLOGY (Dalian) Co., LTD). Reactions
371 included Segment 1:1 cycle of 30 s at 95 °C and Segment 2: 40 cycles of 5 s at 95
372 °C and 20 s at 60 °C. All quantitative PCR assays were performed in duplicate. To
373 provide negative controls and exclude contamination by genomic DNA, the
374 PrimeScript RTEnzyme was omitted in the cDNA synthesis step. To analyze the
375 relative changes in gene expression the 2(-Delta Delta C(T)) method was used.

376

377 **Tissue fixation, immunofluorescence, and confocal imaging**

378 Animals were deeply anaesthetized and subsequently intracardially perfused with
379 4% (weight/vol) paraformaldehyde in 0.1 M phosphate buffer. The brains were
380 dissected out and kept 48 h in 4% paraformaldehyde. Sagittal sections (40 µm)
381 were obtained using a vibratome (Leica VT1000). For immunofluorescence, after
382 blocking/permeabilization (1 h in PBS containing 3 mL/L Triton X-100 and 10 g/L
383 bovine serum albumin (BSA)), sections were incubated overnight with specific
384 antibodies against MAP2 (1:500; SigmaAldrich Cat# M1406, RRID:AB_477171),
385 NeuN (1:500, Millipore Cat# MAB377, RRID:AB_2298772), Parvalbumin
386 (1:1000, Swant Cat# PV27, RID:AB_2631173), GFP FITC-conjugated (1:500,
387 Abcam Cat# ab6662, RRID:AB_305635), Egr1 (1:1000, Cell Signaling Technology
388 Cat# 4154, RRID:AB_2097035) and cFos (1:150, Santa Cruz Biotechnology Cat#
389 sc-52, RRID:AB_2106783). After incubation (2 h) with appropriate fluorescent
390 secondary antibodies (Cy3- or Cy2-coupled fluorescent secondary antibodies,

391 1:200; Jackson ImmunoResearch Labs Cat# 715-165-150, RRID:AB_2340813
392 and Cat# 715545-150, RRID:AB_2340846 respectively), nuclei were stained (10
393 min) with 4',6-diamidino-2-phenylindole (DAPI; catalog #D9542, Sigma-Aldrich).
394 The sections were mounted onto gelatinized slides and cover-slipped with Mowiol.

395

396 **Image analysis and stereological counting**

397 Images (at 1024 × 1024 pixel resolution) in a mosaic format were acquired with a
398 Leica Confocal SP5 with a ×40 oil-immersion or x20 normal objectives and
399 standard (1 Airy disc) pinhole (1 AU) and frame averaging (3 frames per z step)
400 were held constant throughout the study. For pseudo-stereological counting, we
401 analyzed 3 sagittal sections, from 1.4 to 2.0 mm relative to bregma, spaced 300 μm
402 apart. The areas of analysis were, dorsal CA1 and dorsal CA3. Unbiased blind
403 counting of GFP- or MAP2- or Parvalbumin- or NeuN-positive neural cells relative
404 to genotype and condition was performed and normalized to the area of counting.

405

406 **Statistics**

407 Analyses were done using Prism version 8.0.2 for Windows (GraphPad Software,
408 La Jolla, CA, USA). Data are expressed as means ± SEM. Normal distribution was
409 tested with the d'Agostino and Pearson omnibus test. If no difference from
410 normality was detected, statistical analysis was performed using two-tailed
411 Student's *t* test or ANOVA and Tukey's or Dunnett's post-hoc tests. If distribution
412 was not normal, non-parametric two-tailed Mann-Whitney test was used. The
413 $p < 0.05$ was considered as significant.

414

415 **Results**

416 **Differential regulation of gene expression in hippocampus during motor** 417 **learning**

418 Although previous studies implicated individual genes or genetic pathways in
419 learning and memory in the hippocampus, they did not investigate gene expression
420 patterns during motor skill learning. Therefore, to analyze potential changes in
421 hippocampal gene expression during the acquisition of a motor skill we used a
422 transcriptome-scale screening. We subjected two groups of mice to the
423 accelerating rotarod task (Fig. 1A-B). The first group (short-term trained or STT)
424 was trained just one day in the task to assess the initial phase of motor learning,
425 and a second group was trained for five days to acquire well-learned motor skill
426 (long-term trained or LTT). Both groups were compared with mice that were not
427 trained but were placed in the apparatus as a control (non-trained or NT). Twenty-
428 four hours after the last day of training or exposure to the rotarod, the dissected
429 dorsal hippocampus of the mice from the three groups was subjected to deep
430 sequencing analysis (RNAseq).

431 We assessed the overall transcriptional changes in response to training comparing
432 STT vs NT and LTT vs NT (Table 1-1, Adj p-value <0.05; log2fold change > 0.3 or
433 < -0.3). In the comparison of the transcriptional profile between STT and NT we
434 found only two genes that were significantly downregulated in STT compared with
435 NT, *Gsgl1* (an AMPA receptor (AMPA) auxiliary subunit) and *Dusp1*, an
436 inactivator of mitogen-activated protein kinase (MAPK). In contrast, the
437 comparison between LTT and NT revealed that a large number of genes were
438 down- and up-regulated (797 and 540, respectively, Fig.1C). To assess the
439 functional profile of DEGs in the LTT we used enrichment analysis by mapping to
440 Metascape database. We found that downregulated DEGs were significantly
441 enriched in processes related to response to unfolded protein, NOTCH and MAPK
442 pathways (Fig. 1D), whereas upregulated DEGs were DNA recombination, RNA
443 modifications and synaptic organization, structure and activity, particularly in
444 presynaptic processes (Fig. 1D).

445

446 **Ca²⁺ activity decreases in the CA1 pyramidal cells at the end of the motor** 447 **learning task**

448 Hippocampal cell populations are activated during simple locomotion (Bocchio et
449 al., 2020) and during a motor learning task (Albouy et al., 2013). To better
450 understand the hippocampal dynamics during the acquisition of a motor skill, we
451 transduced dorsal CA1 pyramidal cells with AAV-GCaMP6f and we placed a fiber-
452 optic probe to monitor pyramidal neurons activity in CA1 during the accelerating
453 rotarod task (Fig. 2A-C). First, we observed that mice performed well and
454 progressively learned the accelerating rotarod task (Fig. 2D). Interestingly, we
455 observed that during the initial trials of the accelerating rotarod task the Ca²⁺-
456 dependent signal dynamics were irregular and heterogenous whereas at the last
457 trials of the task the signal progressively decreased and stabilized (Fig. 2E-F).
458 Altogether, these results suggest that the pyramidal cells of the CA1 reduce their
459 activity associated with a progressive consolidation of motor learning.

460

461 ***Egr1*-dependent neuronal subpopulations are permanently activated in CA1** 462 **during motor learning**

463 We showed that acquisition and consolidation of motor learning is accompanied
464 by changes in gene expression as well as in Ca²⁺ dynamics. To identify which
465 neural cells are activated during different phases of motor learning, we used a
466 novel mouse line that allows a permanent tagging of neurons activated by
467 experience: the *Egr1*-CreERT2 transgenic mice (Longueville et al., 2021). We
468 chose *Egr1* as promoter because it is a crucial IEG significantly induced in the
469 hippocampus as well as in the cortico-striatal network during initial learning of a
470 motor skill (Hernandez et al., 2006) and it is tightly linked to physiological firing
471 activity of neurons (Vacarino et al., 1992; Wang et al., 1994). Concretely, these
472 mice express the Cre recombinase fused to modified estrogen receptor (ERT2)

473 under the control of the *Egr1* promoter. *Egr1* drives the expression of the CreERT2
474 recombinase that is only active in the presence of tamoxifen metabolite, 4-hydroxy-
475 tamoxifen (4-HT). *Egr1*-CreERT2 mice were crossed with R26^{RCE} mice, a reporter
476 line in which EGFP expression requires recombination by Cre (Fig. 3A).

477 In double transgenic *Egr1*-CreERT² x R26^{RCE} mice, cells in which *Egr1* is induced
478 by neuronal activity and in the presence of 4-HT become permanently labeled with
479 EGFP. We then subjected *Egr1*-CreERT² x R26^{RCE} mice to the accelerating rotarod
480 task using the same three groups (NT, STT, and LTT, Fig 3B). Each group received
481 a single injection of 4-HT 1 h before the last session of training in the task (Fig.
482 3B). To ensure detectable recombination, three days (72 h) after the 4-HT injection,
483 their brains were processed. We then counted the density of GFP-positive neural
484 cells in the CA1 and CA3 of the dorsal hippocampus (Fig. 3C-D). The density of
485 GFP-positive neural cells was increased in CA1 in both, STT and LTT groups
486 compared with NT group whereas they remained unchanged in CA3 (Fig. 3C-D).
487 These results indicated a more sustained *Egr1* activation in a specific group of
488 neuronal cells in CA1 compared with CA3. We then characterized the GFP-positive
489 neural cells in CA1. Co-localization studies revealed that most GFP-positive cells
490 in CA1 were NeuN- and MAP2-positive (and parvalbumin-negative (Fig. 3E-F)
491 indicating they were pyramidal neurons. Finally, we evaluated whether
492 endogenous *Egr1* levels are induced in the dorsal CA1 after STT and LTT. This
493 result was in contrast with *Egr1* mRNA levels in our RNAseq. Specifically, 24 h
494 after the last trial with the rotating rod, *Egr1* expression was reduced only in LTT
495 mice (Gene: *Egr1*, log2 FC: -1,30, adj P value: 6,50E-22; Table 1-1). Altogether
496 suggest a complex and time-dependent regulation of *Egr1* upon motor learning in
497 the rotarod.

498

499 ***Egr1* downstream targets in the hippocampus during motor performance**

500 To evaluate the potential *Egr1*-dependent gene expression, we analyzed in our
501 transcriptome data the differentially expressed genes (DEGs) with *Egr1*-binding
502 motifs in their promoter region (Table 4-1). We identified 1 DEG and 94 DEGs (7
503 % of DEGs in LTT) in STT and LTT respectively which can be regulated by *Egr1*.
504 In particular, *Gsg1l* was a common DEG in STT and LTT compared to NT. Fold-
505 change heatmap (Fig. 4A) shows the genes downregulated and upregulated in
506 LTT with no significant changes observed in STT (Fig. 4A). Interestingly, using the
507 SynGo platform, we identified in this gene data set, 11 genes mapping with
508 processes in synapse assembly, organization and function, and regulation of
509 postsynaptic membrane neurotransmitter receptor levels (Fig. 4A). To further
510 validate these results on a larger number of samples (n = 8 for the NT group, n = 7
511 for the STT group and n= 7 for the LTT group), we performed qPCR analysis on
512 genes *Mdga1*, *Mdga2*, *Gsgl1*, *Arc*, and *Tnik* (Fig.

513 4B-F). We confirmed that the expression of *Mdga1*, *Arc* and *Gsgl1* is reduced in
514 LTT compared with NT group (Fig. 4B-D). Meanwhile, the expression levels of the

515 other two selected genes (*Mdga2* and *Tnik*) showed a trend in increase but these
516 differences were not statistically significant (Fig. 4E-F) which might be explained
517 by the difference in sensitivity of the methods being used. Taken together these
518 data indicate that during the progressive learning of a motor skill, long-term
519 transcriptional changes associated with *Egr1* activity occur in the hippocampus
520 associated with its acquisition and/or maintenance.

521

522 ***Egr1* knockdown in CA1 potentiates motor performance**

523 To test whether *Egr1* levels in the dorsal CA1 control the acquisition and/or
524 maintenance of the motor skills required for the accelerating rotarod task we first
525 evaluated the endogenous levels of *Egr1* during the accelerating rotarod task. We
526 observed that 2 hours after the training with the rotarod, *Egr1* expression was
527 increased in the pyramidal cell layer of the CA1 in both, STT and LTT mice
528 compared with NT mice (Fig. 5A-C). This is in agreement with our ensembles'
529 experiment (Figure 3) which suggests an early upregulation of *Egr1* just after
530 rotarod training, but it is in contrast with the RNAseq 24h after the rotarod (Table
531 1-1) which shows an *Egr1* mRNA levels reduction 24 h later only in the LTT group.
532 Thus, to prove the relevance of the acute *Egr1* increase in the CA1 during motor
533 learning (Fig. 3 and Fig. 5A-C), we transduced the CA1 of wild type (WT) mice with
534 an adeno-associated virus (AAV) expressing a shRNA against the *Egr1* transcript
535 (shRNA-*Egr1* group) or a control shRNA

536 (scramble group) (Fig. 5D-E). After three weeks of viral transduction, we observed
537 a significant reduction of *Egr1* immuno-reactivity in the pyramidal cells of the dorsal
538 CA1 in shRNA-*Egr1* mice compared with the scramble group (Fig. 5F-G). To test
539 the effects of down-regulating *Egr1* in CA1 we subjected the shRNA-*Egr1* and
540 scramble groups of mice to the accelerating rotarod task (Fig. 5H). Scramble mice
541 progressively learned the task and reached a plateau of performance from the
542 second day of training on, whereas, in contrast, the shRNA-*Egr1* mice displayed,
543 from day 3 of training, significant increased latencies to fall from the rotarod
544 compared with the scramble mice (Fig. 5H). These results suggest that *Egr1* down-
545 regulation in the pyramidal neurons of the CA1 improves the accelerating rotarod
546 performance.

547

548 **Depletion of CA1 *Egr1*-dependent neuronal subpopulations enhances motor 549 performance**

550 We observed the activation of *Egr1*-dependent neuronal subpopulations in CA1
551 during the acquisition of motor skills in the accelerating rotarod task and we also
552 showed that a global downregulation of *Egr1* in the dorsal CA1 enhances the
553 performance in this task. We therefore tested the consequences of depleting these
554 CA1 *Egr1*-dependent activated neuronal subpopulations on motor learning to
555 evaluate their contribution. We used the double mutant *Egr1*CreER^{T2} x R26^{RCE}

556 mice (Fig. 6A). These mice were transduced bilaterally in the dorsal CA1 with
557 vehicle or AAV-flex-taCasp3-TEVp (Fig. 6B). Three weeks later, all mice were
558 subjected to the accelerating rotarod task (Fig. 6C) and received an i.p. injection
559 of 4-HT 1 h prior to the training session. This injection was administered at days 1
560 and 2 of the task. With this design, specific *Egr1*-dependent CreER^{T2} induction in
561 activated CA1 pyramidal cells of the CA1 would induce Caspase-3 expression in
562 the presence of 4-HT resulting in cell death of the hippocampal neuronal cells
563 activated in a *Egr1*-dependent fashion. Thus, mice transduced with AAV-flex-
564 taCasp3-TEVp (Casp3 group) in CA1 displayed higher latencies to fall on days 3,
565 4 and 5 compared with control mice (Vehicle group) (Fig. 6C). Brains from these
566 mice were examined to verify the depletion of the *Egr1*-dependent neuronal
567 ensembles (Fig. 6D-E). As expected, mice infused with vehicle in CA1 showed an
568 increase in GFP-positive cells in the pyramidal layer of CA1 after rotarod training
569 when compared with NT mice. In contrast, the density of GFP-positive cells in the
570 dorsal CA1 was dramatically reduced in rotarod-trained mice that were transduced
571 with Casp3 (Fig. 6D-E). This latter result confirmed a depletion of *Egr1*-dependent
572 activated neuronal subpopulations.

573 We also evaluated whether the improvement of Casp3 mice in the rotarod task
574 could be accompanied by a higher activation of neuronal ensembles in the striatum
575 as a compensatory consequence/mechanism of the depletion of *Egr1*-dependent
576 activated neuronal subpopulations. To do so, in the same mice, we analyzed the
577 density of GFP-positive cells in the dorsal striatum (Fig. 6F-G). There was no
578 change in the number of *Egr1*-dependent activated neurons in the dorsal striatum
579 (Fig. 6F-G). Finally, in order to rule out potential leakiness of the *Egr1*-CreER^{T2} x
580 R26^{RCE} mice we repeated the entire experiment but without 4-HT administration.
581 No changes were observed in the rotarod performance in any group as well as no
582 recombination was detected in brains from *Egr1*-CreER^{T2} x R26^{RCE} mice treated
583 with vehicle or AAV-flex-taCasp3-TEVp (Fig. 6H-I). Taken together, our results
584 reinforce the idea of an important role of CA1 *Egr1*-activated pyramidal cells in the
585 modulation of motor skills during an accelerating rotarod task.

586

587 **Chemogenetic activation of CA1 *Egr1*-dependent activated neuronal** 588 **subpopulations impairs motor performance**

589 To further characterize the role of this *Egr1*-dependent neuronal ensemble in CA1
590 induced by motor learning, we used an opposite strategy, aiming to activate it using
591 *designer receptors exclusively activated by designer drugs* (DREADDs)
592 technology. We transduced the dorsal CA1 of *Egr1*-CreER^{T2} mice with an AAV
593 expressing the activator DREADD hM3D(Gq) using a FLEX switch vector (Fig. 7A-
594 B). Three weeks after AAV injection, the mice were first subjected to the
595 accelerating rotarod task (Fig. 7C). On days 1 and 2 of rotarod training, all mice
596 received an injection of 4-HT to induce Cre-mediated recombination in the *Egr1*-
597 expressing neuronal subpopulations. On the last three days of the rotarod task
598 these transduced *Egr1*-dependent cells were activated using clozapine-N-oxide

599 (CNO). The same mice were also tested in the open field (day 7) and novel object
600 location (days 8 and 9, see below). At the end of the study, we tested the efficacy
601 of hM3D(Gq) receptor stimulation by measuring cFos induction in mice treated with
602 CNO or vehicle 2 h before sacrifice and histological analysis (Fig. 7C). Post-
603 mortem histology indicated that CA1 was well targeted with the vector expressing
604 the hM3D(Gq) receptor (Fig. 7D-E). Moreover, CNO induced a robust up-
605 regulation of cFos immunoreactivity in the transduced pyramidal cells in CA1 as
606 compared with non-transduced cells or transduced cells from mice treated with
607 vehicle (Fig. 7F-G).

608 Concerning the rotarod performance, *Egr1-CreERT2* mice transduced with
609 hM3D(Gq) and injected with 4-HT on days 1 and 2, progressively learned the task
610 (Fig. 7H). On days 4, 5 and 6, we treated one group of mice with CNO and the
611 other with vehicle. *Egr1-CreERT2* mice treated with vehicle showed significantly
612 better scores than those treated with CNO in the rotarod performance. The effect
613 became more pronounced at the last day of training (Fig. 7H). To rule out the
614 possibility of unspecific or off-target effects of CNO, we repeated the same
615 experiment as in figure 7H using a new cohort of wild type (WT) mice only treated
616 with CNO or vehicle (Fig. 7I). CNO per se did not induce any effect on the
617 accelerating rotarod performance at any time or session. This result ruled out
618 unspecific off-target effects induced by CNO in motor learning per se. Furthermore,
619 to rule out potential leakiness of the *Egr1CreERT²* mice we repeated in parallel the
620 entire experiment (as in Fig. 7A-H) in a new cohort of mice, but without 4-HT
621 administration. No changes were observed in the rotarod performance in any group
622 as well as no recombination was detected in brains from *Egr1-CreERT²* mice
623 transduced with hM3D(Gq) and treated with vehicle or CNO (Fig. 7J-K).

624 Next, we aimed to assess whether the manipulation of the *Egr1* dependent
625 activated neuronal subpopulations induced during the accelerating rotarod task
626 could affect unspecific and/or general hippocampal-dependent functions such as
627 navigation, anxiety or spatial learning. Thus, we subjected the same *Egr1-CreERT²*
628 mice transduced with hM3D(Gq) receptor (from figure 7) to the open field and novel
629 object location tasks (Fig. 8A). Mice were injected 30 min before the open field test
630 with vehicle or CNO (Fig. 8B). Mice treated with CNO did not display differences
631 in terms of traveled distance (Fig. 8C), time spent in the center (Fig. 8D) and
632 parallel index (Fig. 8E) during the 30 min session in the arena. In the novel object
633 location test, mice treated with CNO showed no modification in new object location
634 preference (Fig. 8F-G). These results show that the alteration of rotarod
635 performance caused by CNO due to the activation of the *Egr1*-dependent neuronal
636 ensemble induced during the accelerating rotarod task was specific.

637

638 Discussion

639 The role of specific brain regions including the striatum, motor cortex and
640 cerebellum in the control of motor learning is well established (De Zeeuw and Ten

641 Brinke, 2015; Giordano et al., 2018; Papale and Hooks, 2018). Less explored is
642 the role of the hippocampus. Potentially, the hippocampus is capable of playing
643 either cooperative or competitive roles during the acquisition of motor skills as
644 suggested by human studies (Poldrack and Packard, 2003; Ghiglieri et al., 2011).
645 However, how the hippocampus is playing such a complex role is puzzling and the
646 underlying cellular and molecular mechanisms remain completely unknown
647 (Albouy et al., 2013). Here we provide evidence for a negative regulation of motor
648 learning implying *Egr1* as a gene controlling a specific subset of pyramidal neurons
649 in the CA1.

650 To our knowledge, our study is the first to profile the transcriptome in the
651 hippocampus following a motor learning task. Our in-depth genome-wide regional
652 comparative study of mRNAs showed that the acquisition of a motor skill involves
653 changes in gene expression particularly during the last phases of the motor
654 learning. This is in line with previous reports showing that the hippocampus shows
655 major structural changes after a long-term training procedure in the accelerating
656 rotarod task (Scholz et al., 2015). Indeed, our cluster and pathway analysis of
657 hippocampal transcriptomic data in response to LTT identified genes related with
658 synapse assembly and organization, regulation of signaling transduction, response
659 to unfolded protein, RNA methylation and DNA recombination which are in turn
660 important processes for formation of hippocampal memories (MacDonald et al.,
661 2006; Svitkina et al., 2010). We observed that the progressive downregulation of
662 the Ca^{2+} signalling in the CA1 pyramidal cells correlated with a progressive
663 improvement of motor learning and with global and changes in gene expression
664 such as a downregulation of genes like *Gsg1l*, *Arc* and *Mdga1*. *Gsg1l* is a novel
665 gene with some roles previously described in the regulation of synaptic activity and
666 plasticity via modulation of AMPA (α -amino-3-hydroxy-5-methyl-
667 4isoxazolepropionic acid) receptors (Coombs et al., 2019). Another couple of
668 interesting genes are *Mdga1* and *Mdga2* which are downregulated and
669 upregulated respectively in long-term trained mice compared with non-trained
670 mice. *Mdga1* is enriched in the hippocampus and its loss has been related with
671 impairments in cognitive skills (Connor et al., 2017). Furthermore, *Mdga1* is a
672 negative regulator of inhibitory synapses (Lee et al., 2013). Therefore, in our
673 trained mice, reduced *Mdga1* levels could be related with an increase of inhibitory
674 activity as observed by our *in vivo* calcium imaging recordings. In contrast,
675 deficiencies in *Mdga2* increases the presence of AMPA receptors in the synaptic
676 membrane and increases excitatory transmission (Connor et al., 2016). In our
677 trained mice, *Mdga2* trends to increase which could result in a decrease of AMPA
678 receptors in the synaptic membrane and a consequent decrease on hippocampal
679 excitatory activity. Notably, among others, *Gsg1l*, *Mdga1* and *Mdga2* are
680 potentially regulated at a transcriptional level by *Egr1*.

681 Here we also demonstrate that, a rapid and early increase of *Egr1* positive
682 ensembles as well as a fast (at 2 hours post training) but transient increase on
683 *Egr1* levels in the CA1 is induced upon motor leaning. However, as shown by gene

684 expression analysis, *Egr1* decreases 24h after LTT suggesting a complex
685 expression pattern depending on the time point on which *Egr1* expression is
686 analysed after the rotarod training. Similar decrease was observed with *Arc*. Such
687 reduction in the abundance of IEG transcripts to levels below the baseline may
688 reflect an active mechanism for transcriptional shut down (Link et al., 1995;
689 Waltereit et al., 2001). Importantly, the subset of hippocampal pyramidal neurons
690 activated by *Egr1* exert a negative regulation on motor learning. This interpretation
691 is indicated by improved learning when these neurons are selectively depleted by
692 Casp3 activation and, on the contrary, impaired rotarod performance when they
693 are chemogenetically stimulated. Moreover, the downregulation of *Egr1* in the
694 hippocampus with shRNA also improved the accelerating rotarod learning
695 performance, indicating a causal role for *Egr1* in these regulations. Thus, our
696 results give support to a role of this CA1 neuronal ensemble as a negative regulator
697 of motor systems giving a molecular/cellular explanation of the phenomena
698 previously suspected in human subjects (Poldrack and Packard, 2003; Ghiglieri et
699 al., 2011). As far as we know, to date there are just a few indirect observations
700 involving *Egr1* with motor-like skills. For example, *Egr1* is induced in the thalamus
701 in motordriven behaviors induced by singing in vocal learning birds (Horita et al.,
702 2012) or in operant conditioning-based tasks in the cortico-striatal pathway
703 (Hernandez et al., 2006) but there is no information about the role of *Egr1* in the
704 procedural motor learning in the rotarod. It is possible that the induced *Egr1*
705 activation in the hippocampus may oppose to the same pathway when activated
706 in other brain regions such as in the striatum. In this line, cocaine-induced
707 hyperlocomotion or extensive instrumental training induced both of them an *Egr1*
708 increase in the striatum (Hernandez et al., 2006; Xu and Kang, 2014). Also, we
709 previously reported in a mouse model of Huntington's disease with severe motor
710 coordination alterations that overexpression of *Rsk1* (a transcription factor) in their
711 striata rescued their motor deficits with a concomitant rescue of their aberrantly
712 reduced *Egr1* levels (Anglada-Huguet et al., 2016).

713 A remarkable phenomenon in our study is that all the manipulations exerted their
714 effects only at the last days of the rotarod training whereas the induction of the
715 *Egr1*-positive engrams was observed in both, the first and the last days of training.
716 This apparent mismatch could be provoked by distinct mechanisms related with
717 short-term and long-term memories (Izquierdo et al., 2002; Cowan, 2008) in which
718 *Egr1*-dependent actions would be only affected by long-term or consolidation or
719 re-activation (Buzsáki, 2015; Giri et al., 2019; Grosmark et al., 2021) mechanisms.
720 Another interpretation is that other systems (striatum, motor cortex, cerebellum)
721 highly involved in the acquisition of motor skills (Turner and Desmurget, 2010; De
722 Zeeuw and Ten Brinke, 2015; Kawai et al., 2015) could compensate for any
723 hippocampal manipulation performed, at least, in the early phases of motor
724 learning.

725 Another intriguing point is that *Egr1*-induction has classically been involved with
726 neuronal activity (Duclot and Kabbaj, 2017), but we observed a decreased

727 hippocampal activity concomitant with Egr1 up-regulation 2 hours after motor
728 learning. This apparent discrepancy could be associated to different phenomena.
729 First, Egr1 is not only involved with enhancement but also with repression of gene
730 expression (Trizzino et al., 2021). Thus, we strongly believe that the underlying
731 transcriptional changes mediated by upregulated Egr1 activity in the particular
732 ensemble would be involved with a long-term and longlasting inhibition of
733 hippocampal neuronal circuits as observed in figure 2. Second, there exist internal
734 loops implying superficial pyramidal cells, deep pyramidal cells and parvalbumin
735 interneurons in the CA1 that could be autoinhibitory (Valero and de la Prida, 2018).
736 Then, it is conceivable that our Egr1-dependent ensemble is labeling such loop
737 although further studies should we performed to demonstrate such statements.
738 Another question raised by this study is the type of information coded by Egr1-
739 dependent neuronal ensembles during motor learning in the hippocampus The
740 hippocampus could play a role in the modulation of anxiety levels related to the
741 task (Cha et al., 2016), or encoding contextual information (Smith and Bulkin,
742 2014) or in the regulation of goal-directed actions in synchrony with the striatum
743 (Albouy et al., 2013; Palombo et al., 2019) and even in the regulation of basal
744 locomotion *per se* (Arriaga and Han, 2017). Thereby, the depletion of the Egr1-
745 dependent neuronal ensemble could eliminate contextual or emotional
746 "distracters" and, therefore, enhance the task performance. Yet it is important to
747 underlie that we did not observe compensatory changes in the striatal activation or
748 major changes in anxiety, locomotion, navigation or spatial learning processes
749 when we manipulated the ensembles induced by the accelerating rotarod task.
750 Alternatively, the activated neurons identified here could code for specific
751 contextual information of the task. However, the hippocampus is capable to create
752 multiple compensatory representations of the same spatial context (Sheintuch et
753 al., 2020). Our study reveals that the molecular mechanism could be driven by
754 Egr1 in a particular group of pyramidal cells of the CA1, which opens the way for
755 further investigation of procedural memory formation.

756

757

758 **Author contributions**

759 V.B. conceived and carried out most experiments, analyzed and interpreted results
760 and wrote the manuscript. E.M. carried out experiments related to fiber photometry.
761 A.S-B. performed and took part in the mRNA and behavioral experiments. A.P.
762 performed and took part in the mRNA and RNAseq experiments. M.M. participated
763 in the discussion and design of the experiments. S.G. discussed the molecular
764 biology experiments. J.A. discussed and supervised histological and
765 morphological experiments. C.M. supervised and designed fiber photometry
766 experiments. J-A.G. supervised and interpreted some parts of the experiments and
767 contributed to the interpretation of data. A.G. conceived and supervised the study,
768 analyzed results and wrote the manuscript.

769

770

771 **References**

- 772 Albouy G, King BR, Maquet P, Doyon J (2013) Hippocampus and striatum:
773 Dynamics and interaction during acquisition and sleep-related motor sequence
774 memory consolidation. *Hippocampus* 23:985–1004.
- 775 Albouy G, Sterpenich V, Baeteu E, Vandewalle G, Deseilles M, Dang-Vu T,
776 Darsaud A, Ruby P, Luppi P-H, Degueldre C, Peigneux P, Luxen A, Maquet P
777 (2008) Both the Hippocampus and Striatum Are Involved in Consolidation of Motor
778 Sequence Memory. *Neuron* 58:261–272.
- 779 Anglada-Huguet M, Giralt A, Rué L, Alberch J, Xifró X (2016) Loss of striatal 90-
780 kDa ribosomal S6 kinase (Rsk) is a key factor for motor, synaptic and transcription
781 dysfunction in Huntington’s disease. *Biochim Biophys Acta - Mol Basis Dis*
782 1862:1255–1266.
- 783 Arriaga M, Han EB (2017) Dedicated Hippocampal Inhibitory Networks for
784 Locomotion and Immobility. *J Neurosci* 37:9222–9238.
- 785 Begeti F, Schwab LC, Mason SL, Barker RA (2016) Hippocampal dysfunction
786 defines disease onset in Huntington’s disease. *J Neurol Neurosurg Psychiatry*
787 87:975–981.
- 788 Bergeron Y, Chagniel L, Bureau G, Massicotte G, Cyr M (2014) mTOR signaling
789 contributes to motor skill learning in mice. *Front Mol Neurosci* 7.
- 790 Berland C et al. (2020) Circulating Triglycerides Gate Dopamine-Associated
791 Behaviors through DRD2-Expressing Neurons. *Cell Metab* 31:773-790.e11.
- 792 Bocchio M, Gouny C, Angulo-Garcia D, Toulat T, Tressard T, Quiroli E, Baude A,
793 Cossart R (2020) Hippocampal hub neurons maintain distinct connectivity
794 throughout their lifetime. *Nat Commun* 11:4559.
- 795 Boutin A, Pinsard B, Boré A, Carrier J, Fogel SM, Doyon J (2018) Transient
796 synchronization of hippocampo-striato-thalamo-cortical networks during sleep
797 spindle oscillations induces motor memory consolidation. *Neuroimage* 169:419–
798 430
- 799 Buzsáki G (2015) Hippocampal sharp wave-ripple: A cognitive biomarker for
800 episodic memory and planning. *Hippocampus* 25:1073–1188.
- 801 Calabresi P, Castrioto A, Di Filippo M, Picconi B (2013) New experimental and
802 clinical links between the hippocampus and the dopaminergic system in
803 Parkinson’s disease. *Lancet Neurol* 12:811–821.
- 804 Camicioli R, Moore MM, Kinney A, Corbridge E, Glassberg K, Kaye JA (2003)
805 Parkinson’s disease is associated with hippocampal atrophy. *Mov Disord* 18:784–
806 790.
- 807 Cha J, Greenberg T, Song I, Blair Simpson H, Posner J, Mujica-Parodi LR (2016)
808 Abnormal hippocampal structure and function in clinical anxiety and comorbid
809 depression. *Hippocampus* 26:545–553.

810 Chagniel L, Bergeron Y, Bureau G, Massicotte G, Cyr M (2014) Regulation of
811 Tyrosine Phosphatase STEP61 by Protein Kinase A during Motor Skill Learning in
812 Mice Fisone G, ed. PLoS One 9:e86988.

813 Connor SA et al. (2016) Altered Cortical Dynamics and Cognitive Function upon
814 Haploinsufficiency of the Autism-Linked Excitatory Synaptic Suppressor MDGA2.
815 Neuron 91:1052–1068.

816 Connor SA, Ammendrup-Johnsen I, Kishimoto Y, Karimi Tari P, Cvetkovska V,
817 Harada T, Ojima D, Yamamoto T, Wang YT, Craig AM (2017) Loss of Synapse
818 Repressor MDGA1 Enhances Perisomatic Inhibition, Confers Resistance to
819 Network Excitation, and Impairs Cognitive Function. Cell Rep 21:3637–3645.

820 Coombs ID, Soto D, McGee TP, Gold MG, Farrant M, Cull-Candy SG (2019)
821 Homomeric GluA2(R) AMPA receptors can conduct when desensitized. Nat
822 Commun 10:4312.

823 Cowan N (2008) Chapter 20 What are the differences between long-term, short-
824 term, and working memory? In, pp 323–338.

825 Curlik DM, Maeng LY, Agarwal PR, Shors TJ (2013) Physical Skill Training
826 Increases the Number of Surviving New Cells in the Adult Hippocampus Smeyne
827 RJ, ed. PLoS One 8:e55850.

828 De Zeeuw CI, Ten Brinke MM (2015) Motor Learning and the Cerebellum. Cold
829 Spring Harb Perspect Biol 7:a021683.

830 DiFeo G, Curlik DM, Shors TJ (2015) The motirod: a novel physical skill task that
831 enhances motivation to learn and thereby increases neurogenesis especially in the
832 female hippocampus. Brain Res 1621:187–196.

833 Dobin A, Davis CA, Schlesinger F, Drenkow J, Zaleski C, Jha S, Batut P, Chaisson
834 M, Gingeras TR (2013) STAR: ultrafast universal RNA-seq aligner. Bioinformatics
835 29:15–21.

836 Döhring J, Stoldt A, Witt K, Schönfeld R, Deuschl G, Born J, Bartsch T (2017)
837 Motor skill learning and offline-changes in TGA patients with acute hippocampal
838 CA1 lesions. Cortex 89:156–168.

839 Duclot F, Kabbaj M (2017) The Role of Early Growth Response 1 (EGR1) in Brain
840 Plasticity and Neuropsychiatric Disorders. Front Behav Neurosci 11.

841 Fidalgo C, Conejo NM, González-Pardo H, Lazo PS, Arias JL (2012) A role for
842 dorsal and ventral hippocampus in response learning. Neurosci Res 73:218–223.

843 Fouquet C, Babayan BM, Watilliaux A, Bontempi B, Tobin C, Rondi-Reig L (2013)
844 Complementary Roles of the Hippocampus and the Dorsomedial Striatum during
845 Spatial and Sequence-Based Navigation Behavior Meck W, ed. PLoS One
846 8:e67232.

847 Ghiglieri V, Sgobio C, Costa C, Picconi B, Calabresi P (2011) Striatum–
848 hippocampus balance: From physiological behavior to interneuronal pathology.
849 Prog Neurobiol 94:102–114.

850 Giordano N, Iemolo A, Mancini M, Cacace F, De Risi M, Latagliata EC, Ghiglieri V,
851 Bellenchi GC, Puglisi-Allegra S, Calabresi P, Picconi B, De Leonibus E (2018)
852 Motor learning and metaplasticity in striatal neurons: relevance for Parkinson’s
853 disease. Brain 141:505–520

854 Giralt A, Sanchis D, Cherubini M, Ginés S, Cañas X, Comella JX, Alberch J (2013)
855 Neurobehavioral characterization of Endonuclease G knockout mice reveals a new
856 putative molecular player in the regulation of anxiety. Exp Neurol 247:122–129.

857 Giri B, Miyawaki H, Mizuseki K, Cheng S, Diba K (2019) Hippocampal Reactivation
858 Extends for Several Hours Following Novel Experience. J Neurosci 39:866–875.

859 Grosmark AD, Sparks FT, Davis MJ, Losonczy A (2021) Reactivation predicts the
860 consolidation of unbiased long-term cognitive maps. Nat Neurosci 24:1574–1585.

861 Harris KL, Armstrong M, Swain R, Erzinclioglu S, Das T, Burgess N, Barker RA,
862 Mason SL (2019) Huntington’s disease patients display progressive deficits in
863 hippocampal-dependent cognition during a task of spatial memory. Cortex
864 119:417–427.

865 Hernandez PJ, Schiltz CA, Kelley AE (2006) Dynamic shifts in corticostriatal
866 expression patterns of the immediate early genes Homer 1a and Zif268 during
867 early and late phases of instrumental training. Learn Mem 13:599–608.

868 Horita H, Kobayashi M, Liu W, Oka K, Jarvis ED, Wada K (2012) Specialized
869 Motor-Driven *dusp1* Expression in the Song Systems of Multiple Lineages of Vocal
870 Learning Birds Vicario DS, ed. PLoS One 7:e42173.

871 Ito R, Robbins TW, Pennartz CM, Everitt BJ (2008) Functional Interaction between
872 the Hippocampus and Nucleus Accumbens Shell Is Necessary for the Acquisition
873 of Appetitive Spatial Context Conditioning. J Neurosci 28:6950–6959.

874 Izquierdo LA, Barros DM, Vianna MRM, Coitinho A, deDavid e Silva T, Choi H,
875 Moletta B, Medina JH, Izquierdo I (2002) Molecular pharmacological dissection of
876 short- and longterm memory. Cell Mol Neurobiol 22:269–287.

877 Kawai R, Markman T, Poddar R, Ko R, Fantana AL, Dhawale AK, Kampff AR,
878 Ölveczky BP (2015) Motor Cortex Is Required for Learning but Not for Executing
879 a Motor Skill. Neuron 86:800–812.

880 Koopmans F et al. (2019) SynGO: An Evidence-Based, Expert-Curated
881 Knowledge Base for the Synapse. Neuron 103:217-234.e4.

882 Lee AS, Duman RS, Pittenger C (2008) A double dissociation revealing
883 bidirectional competition between striatum and hippocampus during learning. Proc
884 Natl Acad Sci 105:17163–17168.

885 Lee K, Kim Y, Lee S-J, Qiang Y, Lee D, Lee HW, Kim H, Je HS, Sudhof TC, Ko J
886 (2013) MDGAs interact selectively with neuroligin-2 but not other neuroligins to
887 regulate inhibitory synapse development. *Proc Natl Acad Sci* 110:336–341.

888 Lerner TN, Shilyansky C, Davidson TJ, Evans KE, Beier KT, Zalocusky KA, Crow
889 AK, Malenka RC, Luo L, Tomer R, Deisseroth K (2015) Intact-Brain Analyses
890 Reveal Distinct Information Carried by SNc Dopamine Subcircuits. *Cell* 162:635–
891 647.

892 Link W, Konietzko U, Kauselmann G, Krug M, Schwanke B, Frey U, Kuhl D (1995)
893 Somatodendritic expression of an immediate early gene is regulated by synaptic
894 activity. *Proc Natl Acad Sci* 92:5734–5738.

895 Longueville S, Nakamura Y, Brami-Cherrier K, Coura R, Hervé D, Girault J (2021)
896 Long-lasting tagging of neurons activated by seizures or cocaine administration in
897 *Egr1-CreER T2* transgenic mice. *Eur J Neurosci* 53:1450–1472.

898 MacDonald JF, Jackson MF, Beazely MA (2006) Hippocampal Long-Term
899 Synaptic Plasticity and Signal Amplification of NMDA Receptors. *Crit Rev*
900 *Neurobiol* 18:71–84.

901 Martín-Ibáñez R, Crespo E, Esgleas M, Urban N, Wang B, Waclaw R,
902 Georgopoulos K, Martínez S, Campbell K, Vicario-Abejón C, Alberch J, Chan S,
903 Kastner P, Rubenstein JL, Canals JM (2012) Helios Transcription Factor
904 Expression Depends on *Gsx2* and *Dlx1&2* Function in Developing Striatal Matrix
905 Neurons. *Stem Cells Dev* 21:2239–2251.

906 Nagai H, de Vivo L, Bellesi M, Ghilardi MF, Tononi G, Cirelli C (2017) Sleep
907 Consolidates Motor Learning of Complex Movement Sequences in Mice. *Sleep* 40.

908 Oliveira AMM, Hawk JD, Abel T, Havekes R (2010) Post-training reversible
909 inactivation of the hippocampus enhances novel object recognition memory. *Learn*
910 *Mem* 17:155–160.

911 Palombo DJ, Hayes SM, Reid AG, Verfaellie M (2019) Hippocampal contributions
912 to valuebased learning: Converging evidence from fMRI and amnesia. *Cogn Affect*
913 *Behav Neurosci* 19:523–536.

914 Papale AE, Hooks BM (2018) Circuit Changes in Motor Cortex During Motor Skill
915 Learning. *Neuroscience* 368:283–297.

916 Poldrack RA, Packard MG (2003) Competition among multiple memory systems:
917 converging evidence from animal and human brain studies. *Neuropsychologia*
918 41:245–251.

919 Schmieder R, Lim YW, Edwards R (2012) Identification and removal of ribosomal
920 RNA sequences from metatranscriptomes. *Bioinformatics* 28:433–435.

921 Scholz J, Niibori Y, W Frankland P, P Lerch J (2015) Rotarod training in mice is
922 associated with changes in brain structure observable with multimodal MRI.
923 *Neuroimage* 107:182–189.

924 Sheintuch L, Geva N, Baumer H, Rechavi Y, Rubin A, Ziv Y (2020) Multiple Maps
925 of the Same Spatial Context Can Stably Coexist in the Mouse Hippocampus. *Curr*
926 *Biol* 30:1467-1476.e6.

927 Sjulson L, Peyrache A, Cumpelik A, Cassataro D, Buzsáki G (2018) Cocaine Place
928 Conditioning Strengthens Location-Specific Hippocampal Coupling to the Nucleus
929 Accumbens. *Neuron* 98:926-934.e5.

930 Smith DM, Bulkin DA (2014) The form and function of hippocampal context
931 representations. *Neurosci Biobehav Rev* 40:52–61.

932 Spargo E, Everall IP, Lantos PL (1993) Neuronal loss in the hippocampus in
933 Huntington's disease: a comparison with HIV infection. *J Neurol Neurosurg*
934 *Psychiatry* 56:487–491.

935 Spiers HJ (2020) The Hippocampal Cognitive Map: One Space or Many? *Trends*
936 *Cogn Sci* 24:168–170.

937 Svitkina T, Lin W-H, Webb DJ, Yasuda R, Wayman GA, Van Aelst L, Soderling SH
938 (2010) Regulation of the Postsynaptic Cytoskeleton: Roles in Development,
939 Plasticity, and Disorders. *J Neurosci* 30:14937–14942.

940 Trizzino M, Zucco A, Deliard S, Wang F, Barbieri E, Veglia F, Gabrilovich D,
941 Gardini A (2021) EGR1 is a gatekeeper of inflammatory enhancers in human
942 macrophages. *Sci Adv* 7 6.

943 Turner RS, Desmurget M (2010) Basal ganglia contributions to motor control: a
944 vigorous tutor. *Curr Opin Neurobiol* 20:704–716.

945 Vaccarino FM, Hayward MD, Nestler EJ, Duman RS, Tallman JF (1992)
946 Differential induction of immediate early genes by excitatory amino acid receptor
947 types in primary cultures of cortical and striatal neurons. *Mol Brain Res* 12:233–
948 241.

949 Valero M, de la Prida LM (2018) The hippocampus in depth: a sublayer-specific
950 perspective of entorhinal–hippocampal function. *Curr Opin Neurobiol* 52:107–114.

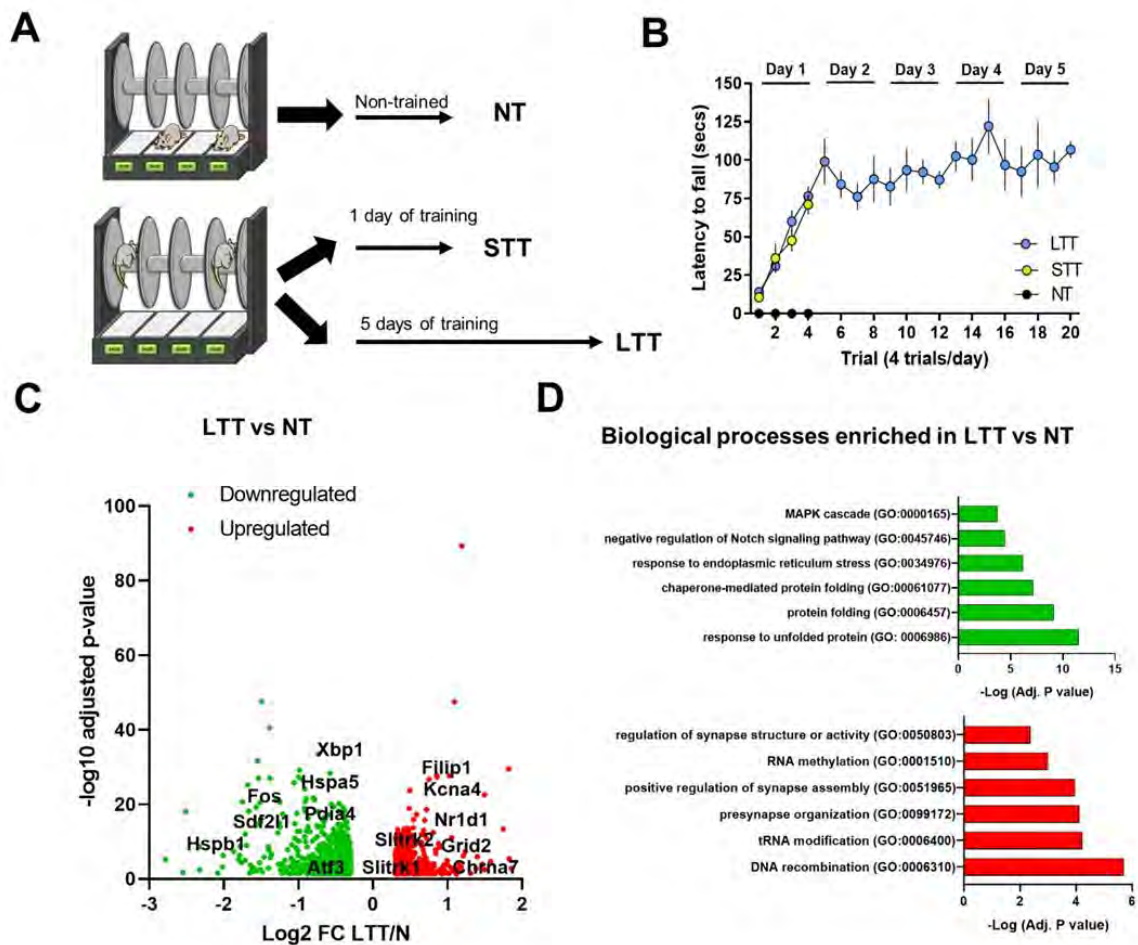
951 Waltereit R, Dammermann B, Wulff P, Scafidi J, Staubli U, Kauselmann G,
952 Bundman M, Kuhl D (2001) Arg3.1/Arc mRNA Induction by Ca²⁺ and cAMP
953 Requires Protein Kinase A and Mitogen-Activated Protein Kinase/Extracellular
954 Regulated Kinase Activation. *J Neurosci* 21:5484–5493.

955 Wang JQ, Daunais JB, McGinty JF (1994) Role of kainate/AMPA receptors in
956 induction of striatal zif/268 and preprodynorphin mRNA by a single injection of
957 amphetamine. *Mol Brain Res* 27:118–126.

958 Xu S, Kang UG (2014) Cocaine induces ubiquitination of Egr-1 in the rat dorsal
959 striatum. *Neuroreport* 25:1362–1367.

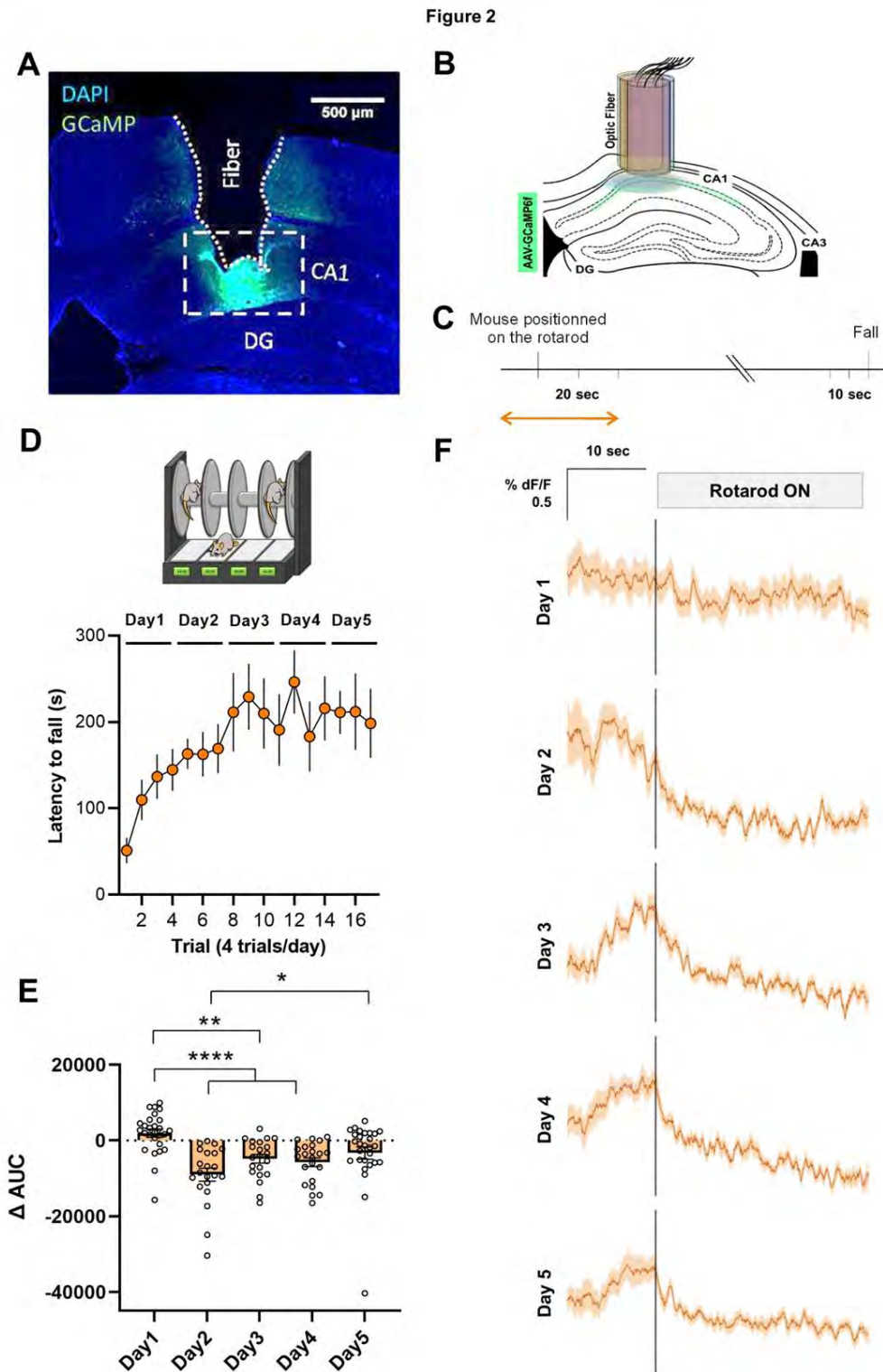
960 Zhou Y, Zhu H, Liu Z, Chen X, Su X, Ma C, Tian Z, Huang B, Yan E, Liu X, Ma L
961 (2019) A ventral CA1 to nucleus accumbens core engram circuit mediates
962 conditioned place preference for cocaine. *Nat Neurosci*.

Figure 1



963

964 **Figure 1.** Hippocampal gene expression profile following the accelerating rotarod
 965 task. **A**, Schematic of experimental design. WT mice were trained on a rotarod.
 966 Three groups were evaluated (n = 5 per group): non-trained (NT), short-term
 967 trained (STT), and long-term trained mice (LTT). The transcriptome of the 5
 968 performers in each group was analyzed by RNA sequencing 24 h after the last
 969 trial. **B**, Latency to fall in the accelerating rotarod task in NT, STT, and LTT mice.
 970 Data are means \pm SEM. **C**, Volcano plots showing significant mRNA differential
 971 expression genes between LTT and NT samples (red: upregulated genes; green:
 972 downregulated genes) (Adj p-value <0.05; log₂FC > 0.3 or < -0.3, n=5 per group).
 973 The name of representative mRNAs is indicated. See extended data table labeled
 974 as Table 1-1 for full data. **D**, Gene ontology analysis for transcriptomic enrichment
 975 of upregulated genes (Upper panel), and downregulated genes in LTT (Lower
 976 panel), by using Metascape analysis including all significant differentially
 977 expressed genes (FDR < 0.05) in LTT.



978

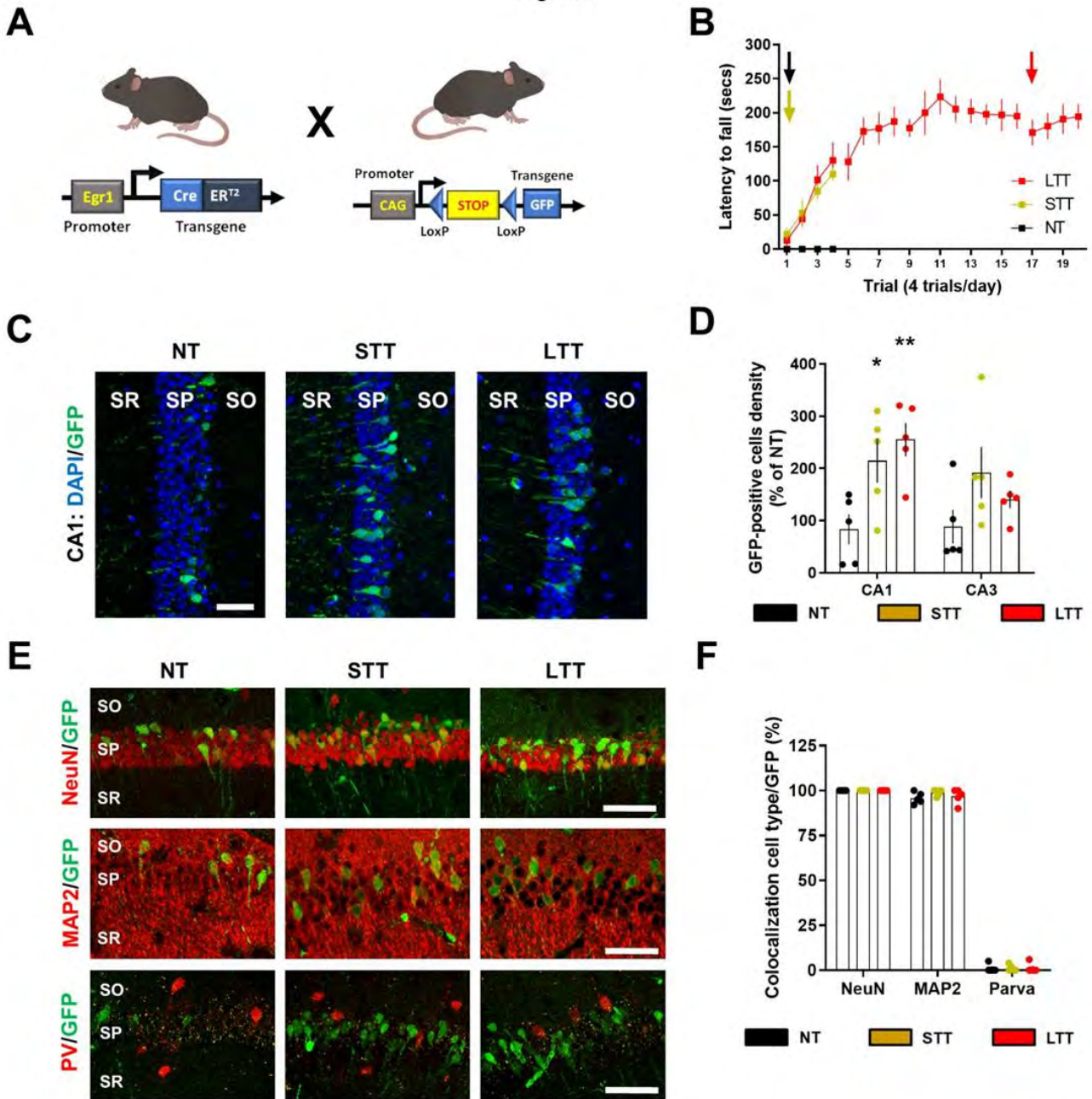
979 **Figure 2.** Accelerating rotarod task induced-functional plasticity in the
 980 hippocampal CA1 neurons. **A**, Representative viral expression of AAVGCaMP6f
 981 and **B**, placement of the fiber-optic probe in CA1 for each mouse depicted in
 982 different colors accordingly. DG, dentate gyrus. **C**, Experimental design of fiber
 983 photometry. Analysis was performed during the time windows indicated by the
 984 orange arrow. **D**, Mice implanted with the fiber-optic probe were subjected to the

985 accelerating rotarod task. **E**, Quantification of the change in the area under the
986 curve (AUC) between [-10, 0 sec] and [0, 10 sec] relative to the placement of the
987 animal in the rotarod. **F**, Averaged traces of GCaMP6f signal expressed as $\Delta F/F\%$
988 for 10 sec before and 20 sec after the mouse was placed on the rotarod. All the
989 trials (n=7 mice) were averaged on each training sessions (days 1 to 5).

990

991

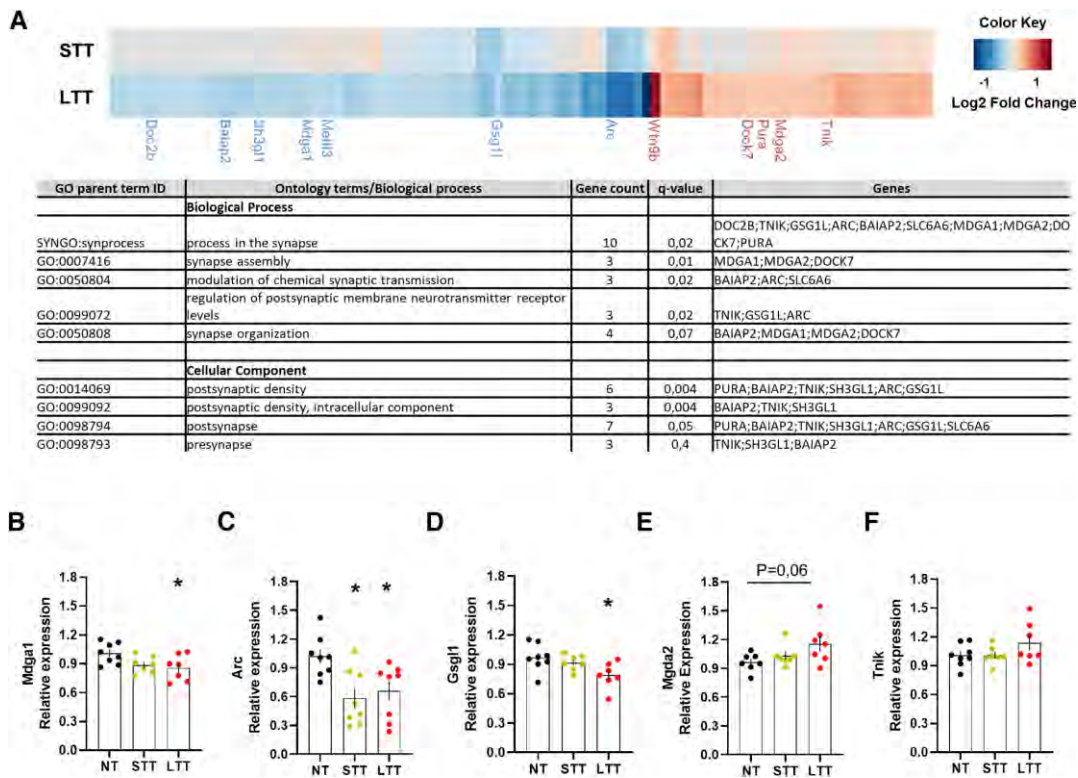
Figure 3



992 **Figure 3.** Characterization of *Egr1*-dependent activated neural cells during
 993 different phases of the rotarod task training. **A**, Schematic representation of the
 994 mutant mice used. **B**, Mice were subjected to three different conditions in an
 995 accelerating rotarod task (as in Fig. 1A): NT, STT, and LTT. All three groups of
 996 mice ($n = 5$ mice per group) received an injection of 4-HT 1 h before the rotarod
 997 training session (arrows) on the last day of training. **C**, Representative images of
 998 *Egr1*-dependent activation of neural cells (GFP-positive, green) co-stained with
 999 DAPI (blue) in dorsal CA1. **D**, Quantification of GFP-positive neural cells density
 1000 per area in NT, STT and LTT groups of mice. Scatter plot with means \pm SEM. Two-
 1001 way ANOVA identified general significant changes between groups ($F_{(2, 88)} = 16.9$;
 1002 $p < 0.0001$). Dunnett's *post hoc* analysis ($* p < 0.05$, $** p < 0.01$) compared with
 1003 the NT group. **E**, Representative images of *Egr1*-dependent activation of neural

1004 cells (GFP-positive, green) co-stained with NeuN or MAP2 or Parvalbumin (all in
1005 red) in CA1. **F**, Quantification of the percentage of GFPpositive neural cells that
1006 co-localizes with various neural markers (in red) in the CA1. PV (Parvalbumin).
1007 CA1-CA3: *cornu ammonis*. SO: *stratum oriens*, SP: *stratum pyramidale*, SR:
1008 *stratum radiatum*. Scale bar in **C** and **E**, 40 μm .

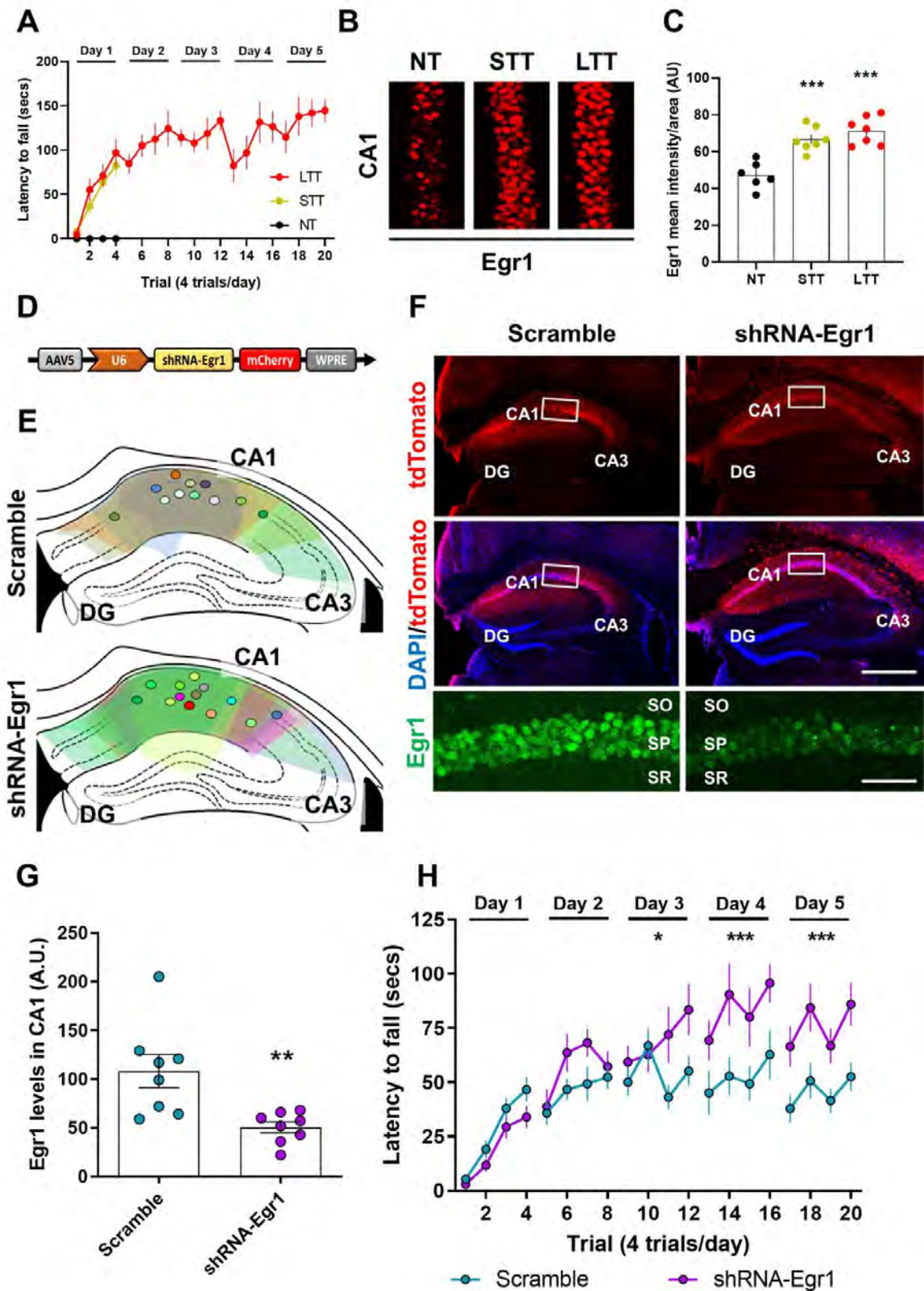
1009



1010

1011 **Figure 4.** Transcriptional changes associated with Egr1 promoter activity
 1012 during the rotarod task training. **A**, Heatmap (upper panel) showing log₂FC
 1013 of DEGs with putative Egr1 binding sites in LTT and STT groups relative
 1014 to the NT group. The results were considered statistically significant at Adj
 1015 p-value <0.05 and log₂FC > 0.3 or < -0.3 in LTT. DEGs in STT are not
 1016 statistically significant except for Gsg1l. Only synaptic genes are named.
 1017 A table (lower panel) is also depicted to show the name of all the putative
 1018 Egr1 binding sites in the LTT group. See extended data table labeled as
 1019 Table 4-1 for full data. Validation of RNA-seq data by quantitative Real-
 1020 Time PCR (qRT-PCR) in NT, STT and LTT groups of mice. Results from
 1021 qRT-PCR performed on a few select genes: **B**, *Mdga1*; **C**, *Arc*; **D**, *Mdga2*;
 1022 **E**, *Gsg1l* and **G**, *Tnik*) enriched in synapse processes. The error bars
 1023 represent the range of the fold change values and data are analyzed by
 1024 one-way ANOVA. A significant difference was detected between groups
 1025 for *Mdga1* ($F_{(2, 19)} = 3,762$; $p < 0.05$), *Arc* ($F_{(2, 21)} = 5,957$; $p < 0.05$) and
 1026 *Gsg1l* ($F_{(2, 19)} = 4,323$; $p < 0.05$). Tukey's post hoc analysis indicated the
 1027 significant differences ($p < 0.05$) compared with the NT group.

Figure 5

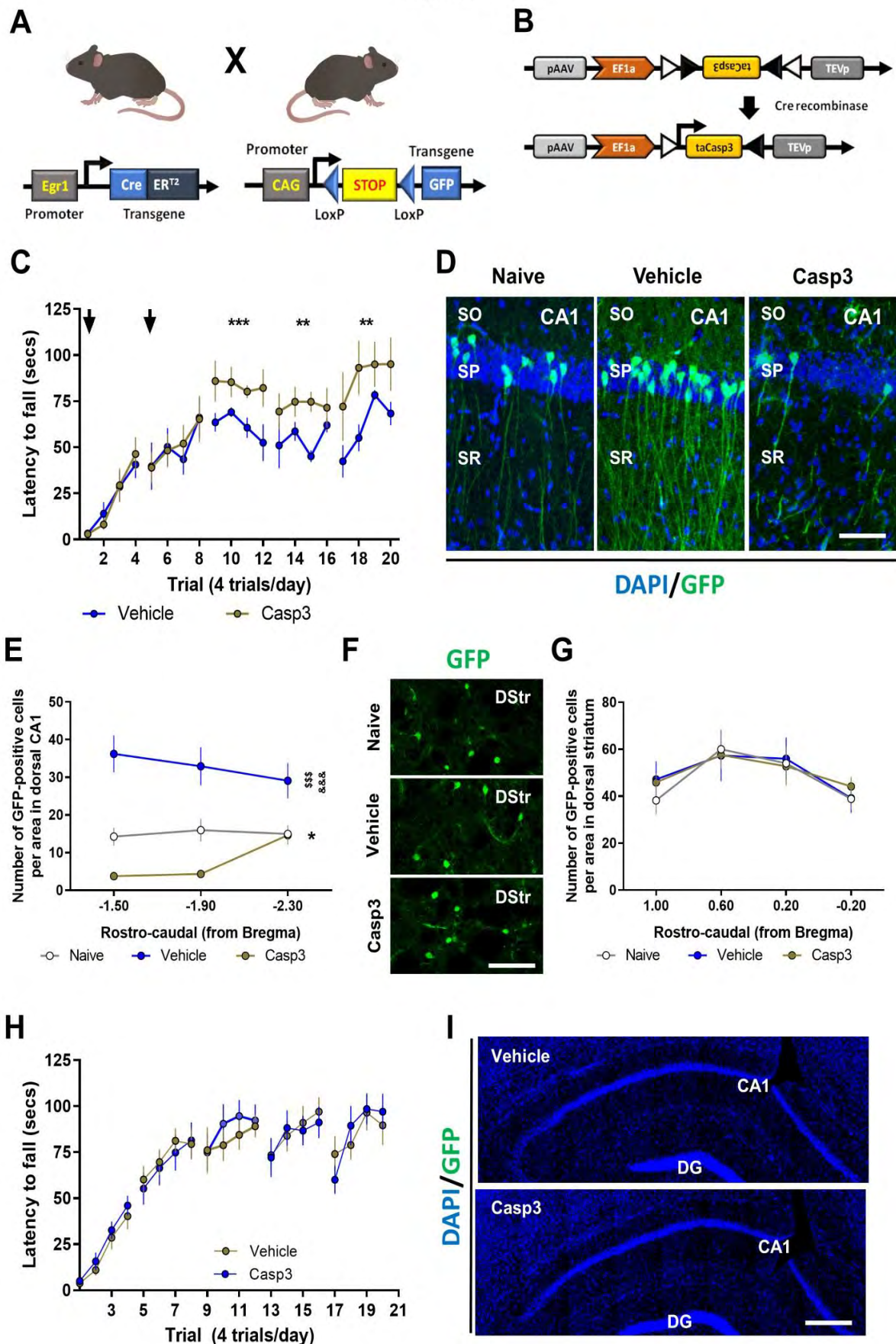


1028

1029 **Figure 5.** Effects of *Egr1* down-regulation in CA1 on accelerating rotarod training.
 1030 **A,** Wild type mice were subjected to three different conditions in an accelerating
 1031 rotarod task as in figure 1: NT, STT, and LTT (4 trials per day). N = 6-7 per group.

1032 **B**, *Egr1* staining (in red) for all three groups 2 hours after the last trial with the
1033 rotarod. **C**, Quantification of *Egr1* optical density (arbitrary units) in the pyramidal
1034 cell layer of CA1. Data are scatter plots (one point per mouse, average from two
1035 slices per mouse) and means \pm SEM. One-way ANOVA ($F_{(2, 17)} = 20.12$, $p =$
1036 0.0001), Dunnet's *post hoc*: *** $p < 0.001$ compared with NT group. **D**, Schematic
1037 illustration of the transduced adeno-associated virus (AAVU6-shRNA-*Egr1*-
1038 mCherry) in a second and new cohort of WT mice. **E**, Schematic location and
1039 distribution of the injection sites in dorsal CA1 for all mice used in this experiment
1040 (only left hemisphere is shown). **F**, Representative images of hippocampi
1041 transduced with control AAV (AAV-U6-Scramble-mCherry, Scramble, left) or with
1042 the experimental AAV (AAV-U6-shRNA-*Egr1*mCherry, shRNA-*Egr1*, right). Triple
1043 staining showing all cells (DAPI, blue), transduced cells (mCherry, red), and *Egr1*-
1044 positive cells (Inset, green) for each group of mice. Scale bars, 300 μm , inset: 60
1045 μm . **G**, Quantification of *Egr1* optical density (arbitrary units) in the pyramidal cell
1046 layer of CA1. Data are scatter plots (one point per mouse, average from two slices
1047 per mouse) and means \pm SEM Mann-Whitney t test, sum of ranks A, 95, B, 41,
1048 Mann-Whitney U, 5, $p = 0.003$, **. N = 8 mice per group. **H**, Three weeks after viral
1049 transduction mice were subjected to the accelerating rotarod task for five days (4
1050 trials per day). N = 11 per group. Data are means \pm SEM and analyzed by two-way
1051 ANOVA. A significant difference was detected between groups on day 3, $F_{(1, 80)} =$
1052 6.30 , $p = 0.0141$), day 4, $F_{(1, 80)} = 16.91$, $p < 0.0001$), and day 5, $F_{(1, 80)} = 26.03$, p
1053 < 0.0001 . DG: Dentate gyrus, CA1: *cornu ammonis* 1, CA3: *cornu ammonis* 3, SO:
1054 *stratum oriens*, SP: *stratum pyramidale*, SR: *stratum radiatum*.

Figure 6



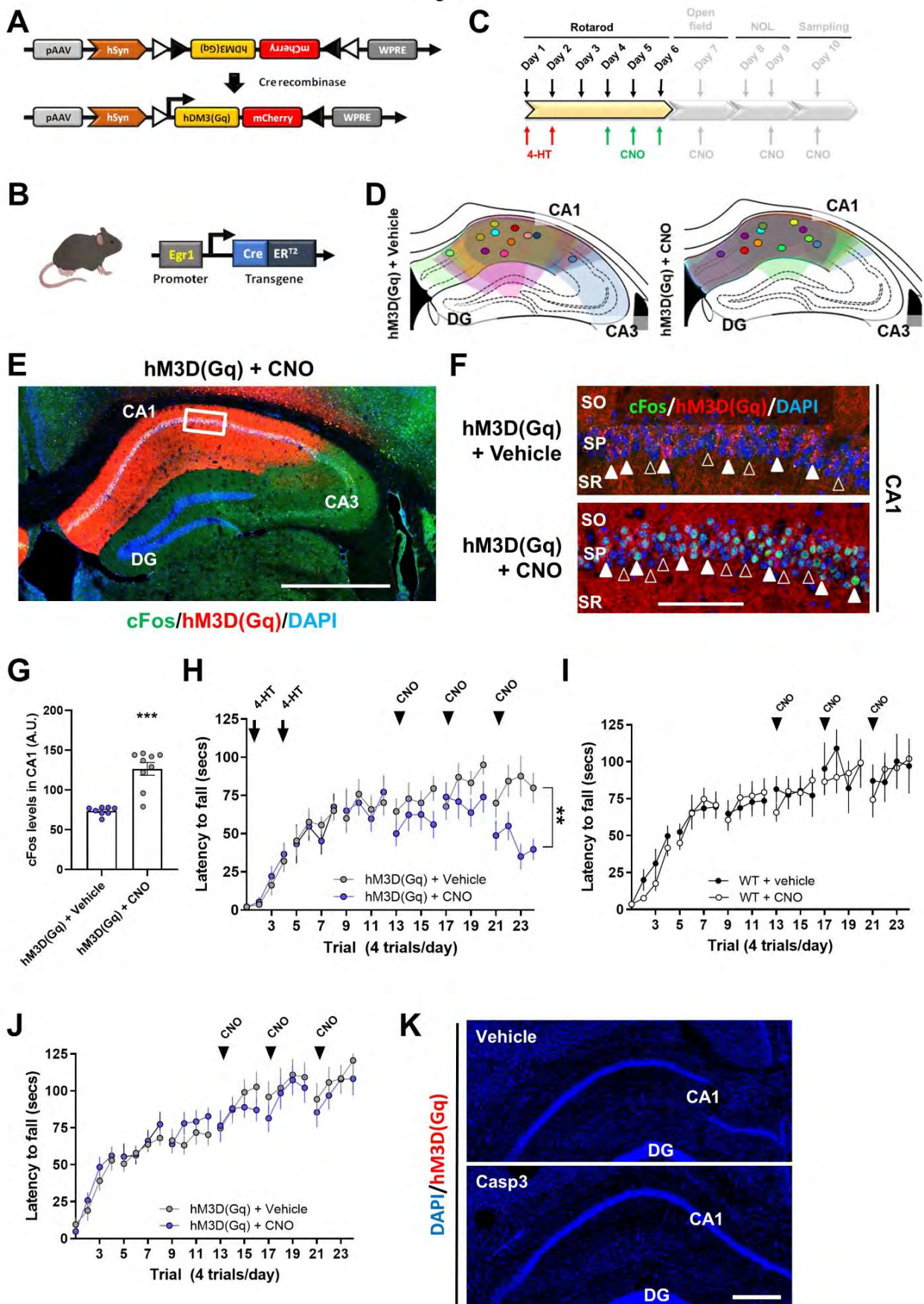
1055 **Figure 6.** Depletion of the CA1 Egr1-dependent activated neurons during the
 1056 rotarod task. **A**, Schematic representation of the double mutant mice used in this
 1057 experiment. **B**, Schematic representation of the AAV-flex-taCasp3-TEVp vector.
 1058 Mice were bilaterally injected in CA1 with AAV-flex-taCasp3-TEVp (Casp3, n = 8)

1059 or vehicle (Vehicle, n = 7). A group of non-trained mice (Naive, n = 5) was also
1060 used. **C**, All three groups received a single injection 4-HT 1 h prior to the rotarod
1061 training (arrows) on days 1 and 2 of training. Data are means \pm SEM, analyzed by
1062 two-way ANOVA. A significant difference was detected between groups on day 3,
1063 $F_{(1, 52)} = 15.78$, $p = 0.0002$; day 4, $F_{(1, 52)} = 9.9588$, $p = 0.0027$; and day 5, $F_{(1, 52)} =$
1064 10.05 , $p = 0.0025$. **D**, Representative images of *Egr1*-dependent activation of
1065 neural cells (GFP-positive, green) co-stained with DAPI (blue) in the dorsal CA1 of
1066 the hippocampus in the three groups. Scale bar, 60 μ m. **E**, Quantification of
1067 hippocampal GFP-positive neural cells density per area in the three groups. Data
1068 are means \pm SEM. Two-way ANOVA identified general significant changes
1069 between groups, $F_{(2, 51)} = 49.27$, $p < 0.0001$. Tukey's *post hoc* analysis indicated
1070 that both, Naive ($p < 0.05$) and Casp3 ($p < 0.001$) showed significantly different
1071 GFP-positive cell density compared with Vehicle mice. *: Naive vs Vehicle groups;
1072 §: Casp3 vs Naive; &: Casp3 vs Vehicle. **F**, Representative images of *Egr1*-
1073 dependent activation of neural cells (GFP-positive, green) in the dorsal striatum
1074 (DStr) from the three groups. Scale bar, 120 μ m. **G**, Quantification of striatal GFP-
1075 positive neural cells density per area in the three groups. **H**, A new cohort of double
1076 mutant mice as in **A**, were subjected to the same experimental design as in **B-C**
1077 but without 4-HT administration to rule out potential leakiness of the system. Data
1078 are means \pm SEM, analyzed by two-way ANOVA (no significant differences were
1079 detected between groups) **I**, Post-mortem hippocampal examination in mice from
1080 **H** shows no recombination due to the absence of 4-HT administration. SO: *stratum*
1081 *oriens*, SP: *stratum pyramidale*, SR: *stratum radiatum*.

1082

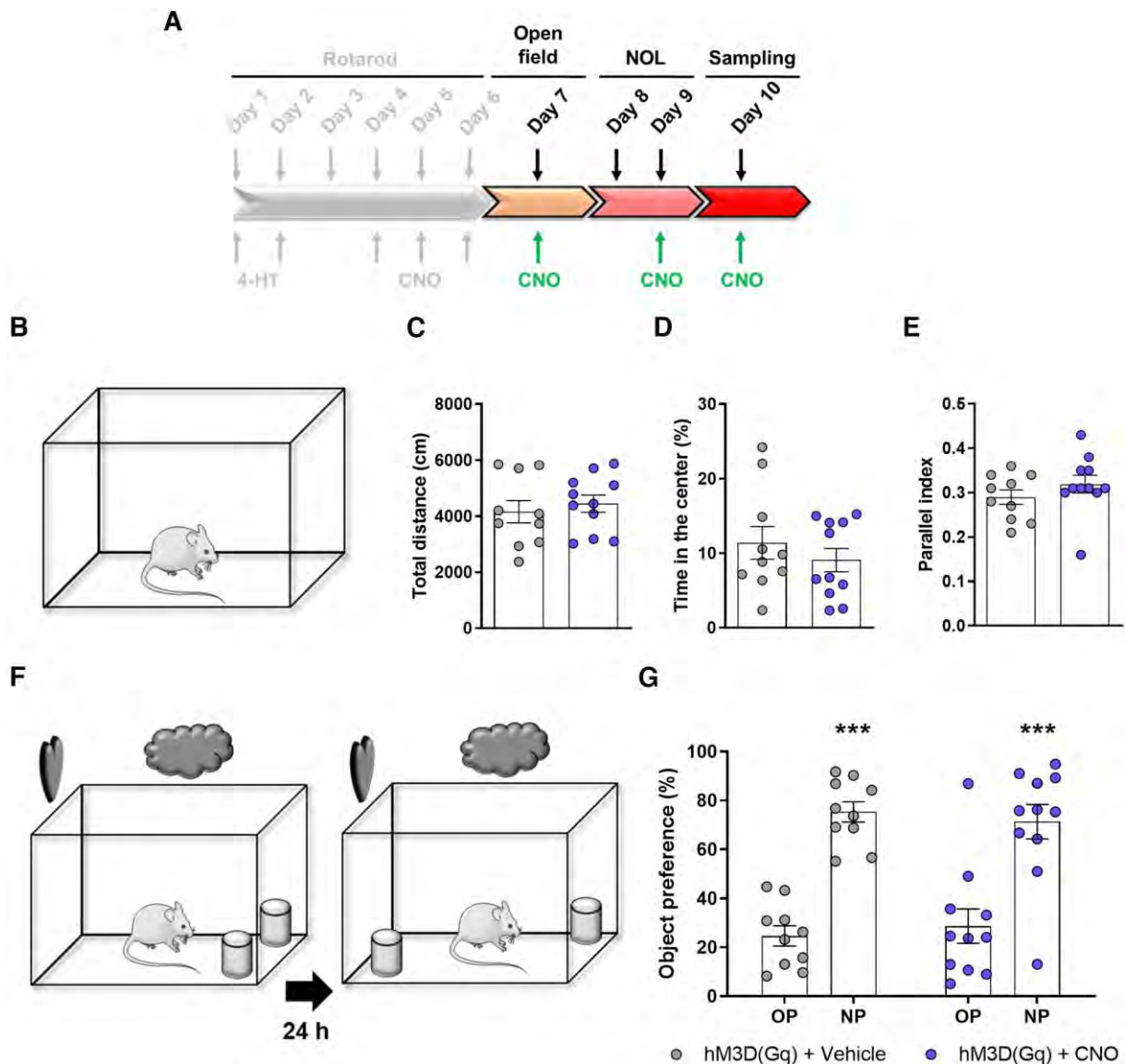
1083

Figure 7



1084 **Figure 7.** Effects of chemogenetic activation of the CA1 Egr1-dependent activated
 1085 neurons during the rotarod task. **A**, Design of the AAV vector to express hM3D(Gq)
 1086 only in cells with Cre recombinase activity. **B**, Egr1-CreER^{T2} mutant mice used. **C**,
 1087 Scheme depicting the behavioral characterization in the present figure (colored).
 1088 **D**, Schematic location of the injection site for each mouse (only left hemisphere is

1089 shown). **E**, Representative image of a transduced hippocampus from a mouse
1090 treated with CNO. **F**, Representative images of CA1 in mice from **E**. Empty
1091 arrowheads designate non-transduced cells, white arrowheads designate
1092 transduced cells. **G**, Quantification of cFos immunofluorescence intensity in the
1093 CA1 pyramidal cell layer of transduced mice and treated with 4-HT and Vehicle (n
1094 = 8) or CNO (n = 9). Means \pm SEM Mann-Whitney t test (sum of ranks A, 36, B,
1095 117, U = 0, $p < 0.0001$). **H**, Accelerating rotarod task in transduced mice. Arrows
1096 indicate treatment with 4HT and arrowheads treatment with CNO. Data are means
1097 \pm SEM. Two-way ANOVA identified significant differences between groups on last
1098 day of training ($F_{(1, 76)} = 26,41$, $p < 0.0001$). **I** Two independent groups of WT mice
1099 treated with vehicle (n = 10) or CNO (3 mg/kg, n = 11) respectively were subjected
1100 to the accelerating rotarod task with the same design as in **H**. **J**, A new cohort of
1101 mutant mice as in **B**, were subjected to the same experimental design as in **A-C**
1102 but without 4-HT administration to rule out potential leakiness of the system. Data
1103 are means \pm SEM, analyzed by two-way ANOVA (no significant differences were
1104 detected between groups). **K**, Post-mortem hippocampal examination in mice from
1105 **J** shows no recombination due to the absence of 4-HT administration. Data are
1106 means \pm SEM Scale bar in **E**, 300 μ m, in **F**, 60 microns and in **K**, 100 microns. DG:
1107 *dentate gyrus*, CA1: *cornu amonis 1*, CA3: *cornu amonis 3*, SO: *stratum oriens*,
1108 SP: *stratum pyramidale*, SR: *stratum radiatum*.



1109

1110 **Figure 8.** Chemogenetic modulation of the CA1 Egr1-dependent activated
 1111 neurons does not alter performance in other hippocampal-related tasks. **A**, After
 1112 the accelerating rotarod task showed in figure 7A-H (gray tone scheme), the Egr1-
 1113 CreER^{T2} mutant mice transduced with AAV-hSYN-DIO-hM3D(Gq)-mCherry
 1114 construct and treated with 4HT at the beginning of the rotarod training (see Fig. 7)
 1115 were subjected to hippocampal-related tasks. Thirty min before open field task and
 1116 before the testing session in the NOL task, all mice received a single i.p. injection
 1117 of vehicle (n = 10) or CNO (3 mg/kg, n = 11). In the open field task **B**, CNO injection
 1118 effects on the total distance travelled **C**, the time spent in the center of the arena
 1119 **D** and the parallel index **E** are shown. Unpaired t test in **D** and **E** or Mann-Whitney
 1120 t test in **G** did not detect significant differences between groups in any parameter.
 1121 **F**, In the novel object location test, CNO injection effects on the novel object
 1122 location preference are shown **G**. Two-way ANOVA identified significant and equal
 1123 novel object location preference (Novel object location preference effect: $F_{(1, 38)} =$
 1124 $62,11, p < 0.0001$) but no differences were found between groups (Group effect:

1125 $F_{(1, 38)} = 1,9 \cdot 10^{-14}$, $p = 0.99$). OP: Old position, NP: New position. In **C**, **D**, **E** and **G**
1126 data are individual values for every mouse and means \pm SEM are shown.

1127 **Table 1-1.** Hippocampal differentially expressed genes in STT and LTT groups
1128 compared with NT group. Table 1-1 is supporting figure 1 results. Differentially
1129 expressed genes (upregulated or downregulated; Adj p-value <0.05; log2fold
1130 change > 0.3 or < -0.3) in pair comparisons are depicted as follows: NT vs STT
1131 groups; NT vs LTT groups.

1132

1133 **Table 4-1.** Differentially expressed genes with potential regulation by Egr1.
1134 Differentially expressed genes (upregulated or downregulated; Adj p-value <0.05;
1135 log2fold change > 0.3 or < -0.3) with Egr1-binding motifs in their promoter region
1136 obtained by pair comparisons are depicted comparing NT vs LTT groups.